Appl Phys B (2010) 101: 143–165
DOI 10.1007/s00340-010-4182-8

Applied Physics B
Lasers and Optics

Superluminal spectral densities of ultra-relativistic electrons in intense electromagnetic wave fields

R. Tomaschitz

Received: 25 January 2010 / Revised version: 12 July 2010 / Published online: 27 August 2010

Abstract Superluminal radiation from electrons accelerated in electromagnetic waves is investigated. The radiation field is a Proca field with negative mass-square, minimally coupled to the electron current. The spectrum is continuous in the ultra-relativistic regime, where steepest-descent asymptotics can be used to evaluate the power coefficients. The time averaging of Lissajous orbits in polarized wave fields is discussed, and the tachyonic spectral densities of electrons orbiting in intense laser beams are derived. In the ultra-relativistic limit, realized by high injection energy or high field intensity, the spectral functions are evaluated in closed form in terms of Airy integrals. In contrast to electromagnetic radiation, there is a longitudinal polarization component, and oscillations emerge at high beam intensity in the longitudinal and transversal spectral slopes, generated by the negative mass-square of the tachyonic quanta. The thermal ultra-relativistic electron plasma of two active galactic nuclei is analyzed in this regard, based on TeV spectral maps obtained with imaging air Cherenkov detectors. Specifically, tachyonic cascade fits are performed to γ-ray flares of the TeV blazars RGB J0152 + 017 and 3C 66A, and the transversal and longitudinal radiation components are disentangled in the spectral maps. The curvature of the spectral slopes is shown to be intrinsic, caused by the Boltzmann factor of the electronic source plasma radiating the tachyonic cascades.

1 Introduction

We study the effect of acceleration on the superluminal spectral densities of electrons orbiting in electromagnetic waves. The tachyonic radiation field is a Proca field with negative mass-square coupled to a subluminal current. The Lagrangian reads

$$L_{\text{Proca}} = -\frac{1}{4}F_{\alpha\beta}F^{\alpha\beta} + \frac{1}{2}m_{\text{t}}^2 A_\alpha A^\alpha + A_\alpha j^\alpha,$$
$$j^0 = \rho = q\delta\big(\mathbf{x} - \mathbf{x}(t)\big), \quad \mathbf{j} = q\mathbf{v}\delta\big(\mathbf{x} - \mathbf{x}(t)\big), \tag{1.1}$$

where m_{t} is the mass of the superluminal Proca field A_α with field tensor $F_{\alpha\beta} = A_{\beta,\alpha} - A_{\alpha,\beta}$, and q the tachyonic charge carried by the current j^α. The mass term in the Lagrangian is added with a positive sign, and the sign convention for the metric is diag$(-1, 1, 1, 1)$, so that $m_{\text{t}}^2 > 0$ is the negative mass-square of the radiation field. Tachyonic radiation implies superluminal signal transfer [1–7], the energy quanta propagating faster than light in vacuum, in contrast to rotating superluminal light sources emitting vacuum Cherenkov radiation [8, 9]. This superluminal energy propagation by tachyonic vacuum modes is also to be distinguished from superluminal group velocities arising in photonic crystals, microcavity waveguides, and optical fibers [10–14]. In contrast to tachyonic quanta, the actual signal speed defined by the electromagnetic energy flow in these media is subluminal and occasionally even opposite to the group velocity. Here, we derive the radiation densities of ultra-relativistic electrons accelerated in electromagnetic plane waves [15, 16]; tachyonic spectral densities generated by uniformly moving charges have been discussed in [17–20].

The existence of superluminal energy transfer has not been established so far, and one may ask why. There is the possibility that superluminal quanta just do not exist,

R. Tomaschitz (✉)
Department of Physics, Hiroshima University, 1-3-1
Kagami-yama, Higashi-Hiroshima 739-8526, Japan
e-mail: tom@geminga.org
Fax: +81-824-240717

the vacuum speed of light being the definitive upper bound. There is another explanation, the interaction of superluminal radiation with matter is very small, the quotient of tachyonic and electric fine-structure constants being $q^2/e^2 \approx 1.4 \times 10^{-11}$ [5], and therefore superluminal quanta are hard to detect. There have been searches for superluminal particles, which were assumed to be electrically charged sources of vacuum Cherenkov radiation [2], and bubble-chamber events were reanalyzed in search of negative mass-squares inferred from energy-momentum conservation [3, 4].

Here, we investigate superluminal radiation by electrons in ultra-intense laser beams and from ultra-relativistic electron plasmas [21–23]. The negative mass-square of the tachyonic radiation field results in a longitudinal radiation component, and the acceleration the electron undergoes in a laser beam generates oscillations along the slopes of the spectral densities. For the spectrum to be continuous, ultra-relativistic electronic Lorentz factors are required, generated by high injection energies and/or electromagnetic wave fields of high intensity. The superluminal radiation densities of ultra-relativistic electrons accelerated in a polarized electromagnetic plane wave can be expressed in closed form by means of Airy functions depending on the Stokes parameters, wavelength, and intensity of the electromagnetic wave, all combined in a single spectral variable in the ultra-relativistic limit. Tachyonic cascade spectra are obtained by averaging the superluminal spectral densities with ultra-relativistic electron distributions. The thermodynamic parameters of the electron plasma as well as the transversal and longitudinal flux components can be inferred from the cascade fit.

In particular, we perform tachyonic cascade fits to γ-ray flare spectra of two TeV blazars, the BL Lacertae objects (BL Lacs) RGB J0152 + 017 [24] and 3C 66A [25, 26], and extract the thermodynamic parameters of the electron plasma in the galactic nuclei. In contrast to GeV–TeV photons, the extragalactic tachyon flux is not attenuated by the cosmic background light, as tachyons cannot interact with infrared background photons. By comparing to the spectral maps of other BL Lacs, we show that the curvature in the GeV–TeV spectra of blazars is a consequence of the Boltzmann factor of the thermal electron plasma in the active galactic nuclei. The spectral curvature is reproduced by the superluminal cascades without resort to intergalactic attenuation mechanisms. In the spectral map of blazar 3C 66A, an extended spectral plateau typical for tachyonic γ-ray spectra emerges in the high MeV and low GeV range [27, 28].

In Sect. 2, we set up the general formalism, deriving the tachyonic Poynting vectors and the transversal and longitudinal power coefficients. In Sect. 3 and Appendix C, we calculate the superluminal spectral densities of ultra-relativistic electrons orbiting in polarized electromagnetic waves. In Sect. 4.1, we consider ultra-intense laser fields, and study the effect of polarization on the tachyonic radiation densities of electrons injected into the laser beam. In Sect. 4.2, we discuss tachyonic cascade spectra generated by the thermal ultra-relativistic electron plasmas of active galaxies, and show how to disentangle the polarization components in the spectral maps. The conclusions are summarized in Sect. 5. In Appendices A and B, we enumerate the different types of trajectories in polarized wave fields, and explain the time averaging of Lissajous orbits in electromagnetic plane waves.

2 Superluminal flux vectors and power coefficients

We start with the current density $\mathbf{j}(\mathbf{x}, t)$ generated by a charge in arbitrary motion. The truncated Fourier representation of the current reads

$$\hat{\mathbf{j}}(\mathbf{x}, \omega) = \int_{-T/2}^{+T/2} \mathbf{j}(\mathbf{x}, t) \mathrm{e}^{\mathrm{i}\omega t}\, \mathrm{d}t, \tag{2.1}$$

and we define the truncated delta functions

$$\begin{aligned} \delta_{(1)}(\omega; T) &:= \frac{1}{2\pi} \int_{-T/2}^{+T/2} \mathrm{e}^{\mathrm{i}\omega t}\, \mathrm{d}t, \\ \delta_{(2)}(\omega; T) &:= \frac{2\pi}{T} \big(\delta_{(1)}(\omega; T)\big)^2, \end{aligned} \tag{2.2}$$

both of which are limit definitions of the Dirac function, $\delta_{(1,2)}(\omega; T \to \infty) = \delta(\omega)$. In this way, a well-defined meaning is given to squares of delta functions arising in the tachyonic flux vectors. The latter are based on the current transform, see (2.1),

$$\begin{aligned} \hat{\mathbf{J}}(\mathbf{x}, \omega) &:= \int \mathrm{d}\mathbf{x}' \hat{\mathbf{j}}(\mathbf{x}', \omega) \exp\big(-\mathrm{i}k(\omega)\mathbf{n}\mathbf{x}'\big), \\ k(\omega) &:= \operatorname{sign}(\omega)\sqrt{\omega^2 + m_\mathrm{t}^2}, \end{aligned} \tag{2.3}$$

where $k(\omega)$ is the tachyonic wave number and $m_\mathrm{t} > 0$ the tachyon mass. The projection of $\hat{\mathbf{J}}(\mathbf{x}, \omega)$ onto a right-handed triad of polarization vectors $\boldsymbol{\varepsilon}_{1,2}$ and $\mathbf{n}$ of the tachyonic radiation field reads

$$\begin{aligned} \hat{\mathbf{J}}^{\mathrm{T}(j)}(\mathbf{x}, \omega) &:= \boldsymbol{\varepsilon}_j(\mathbf{x})\big(\boldsymbol{\varepsilon}_j(\mathbf{x})\hat{\mathbf{J}}(\mathbf{x}, \omega)\big), \\ \hat{\mathbf{J}}^{\mathrm{T}}(\mathbf{x}, \omega) &:= \hat{\mathbf{J}}^{\mathrm{T}(1)}(\mathbf{x}, \omega) + \hat{\mathbf{J}}^{\mathrm{T}(2)}(\mathbf{x}, \omega), \\ \hat{\mathbf{J}}^{\mathrm{L}}(\mathbf{x}, \omega) &:= \mathbf{n}\big(\mathbf{n}\hat{\mathbf{J}}(\mathbf{x}, \omega)\big), \quad \hat{\mathbf{J}} = \hat{\mathbf{J}}^{\mathrm{T}} + \hat{\mathbf{J}}^{\mathrm{L}}. \end{aligned} \tag{2.4}$$

Here, $\mathbf{n} := \mathbf{x}/|\mathbf{x}|$ is the coordinate unit vector identified as longitudinal polarization vector, and $\boldsymbol{\varepsilon}_{1,2}$ are real transversal polarization vectors defining two degrees of linear polarization, so that $\boldsymbol{\varepsilon}_1$, $\boldsymbol{\varepsilon}_2$ and $\mathbf{n}$ constitute an orthonormal triad.

We consider a subluminal particle $\mathbf{x}_0(t)$ moving in the vicinity of the coordinate origin. The particle carries a tachyonic charge q, resulting in the charge and current densities

$j^0 = \rho = q\delta(\mathbf{x} - \mathbf{x}_0(t))$ and $\mathbf{j}(\mathbf{x}, t) = q\dot{\mathbf{x}}_0\delta(\mathbf{x} - \mathbf{x}_0(t))$, so that

$$\hat{\mathbf{J}}(\mathbf{x}, \omega; T) = q\int_{-T/2}^{+T/2} \exp\bigl[-\mathrm{i}\bigl(k(\omega)\mathbf{n}\mathbf{x}_0(t) - \omega t\bigr)\bigr]\,\mathrm{d}\mathbf{x}_0(t), \tag{2.5}$$

where $\mathbf{n}$ coincides with the unit wave vector of the outgoing spherical waves. In this representation, the trajectory can also be used if parametrized by a variable φ other than time, without the need of inversion. We then use $\mathbf{x}_0(\varphi)$ and $t(\varphi)$ in the exponential, and replace the integration over $\mathrm{d}\mathbf{x}_0(t)$ by $\mathrm{d}\mathbf{x}_0(\varphi)$, with integration boundaries $\varphi(\pm T/2)$. In this case, we use a slightly modified form of the truncated delta functions in (2.2), adapted to the φ parametrization. We define $T_\varphi := \varphi(T/2) - \varphi(-T/2)$, where $\varphi(t)$ is the inverse of $t(\varphi)$, and

$$\begin{aligned} \delta_{(1)}(\omega; T_\varphi) &:= \frac{1}{2\pi}\int_{\varphi(-T/2)}^{\varphi(T/2)} \mathrm{e}^{\mathrm{i}\omega\varphi}\,\mathrm{d}\varphi, \\ \delta_{(2)}\bigl(\omega; |T_\varphi|\bigr) &:= \frac{2\pi}{|T_\varphi|}\bigl(\delta_{(1)}(\omega; T_\varphi)\bigr)^2, \end{aligned} \tag{2.6}$$

so that $\delta_{(1,2)}(\omega; |T_\varphi| \to \infty) = \delta(\omega)$.

The time-averaged asymptotic Poynting vectors read [6],

$$\begin{aligned} \bigl\langle \mathbf{S}^{\mathrm{T}(j)}\bigr\rangle &\sim \frac{\mathbf{n}}{4(2\pi)^4 r^2}\frac{2\pi}{T}\int_{-\infty}^{+\infty} \omega k(\omega)\bigl|\hat{\mathbf{J}}^{\mathrm{T}(j)}(\mathbf{x}, \omega; T)\bigr|^2\,\mathrm{d}\omega, \\ \bigl\langle \mathbf{S}^{\mathrm{L}}\bigr\rangle &\sim \frac{\mathbf{n}}{4(2\pi)^4 r^2}\frac{2\pi}{T}m_\mathrm{t}^2\int_{-\infty}^{+\infty} \frac{k(\omega)}{\omega}\bigl|\hat{\mathbf{J}}^{\mathrm{L}}(\mathbf{x}, \omega; T)\bigr|^2\,\mathrm{d}\omega, \end{aligned} \tag{2.7}$$

with $k(\omega) = \mathrm{sign}(\omega)\sqrt{\omega^2 + m_\mathrm{t}^2}$ as defined in (2.3); the sign change enters due to the Fourier representation stretching symmetrically over positive and negative frequencies. The wave number changes its sign when the frequency does, so that waves labeled by ±ω are equivalent, propagating into the same direction; negative frequencies are used for notational convenience only. Squared absolute values of complex vectors always imply complex conjugation, $|\hat{\mathbf{J}}|^2 := \hat{\mathbf{J}}\hat{\mathbf{J}}^*$. The total transversal flux $\langle \mathbf{S}^\mathrm{T}\rangle$ is obtained by adding the transversal polarization components $\langle \mathbf{S}^{\mathrm{T}(j)}\rangle$, or by substituting $\hat{\mathbf{J}}^\mathrm{T}$ into the integrand instead of the linearly polarized current transforms $\hat{\mathbf{J}}^{\mathrm{T}(j)}$, see (2.4). The radiant power in the respective polarization is obtained by integrating the flux through a sphere of radius $r \to \infty$,

$$P^{\mathrm{T}(j),\mathrm{L}} = r^2\int \bigl\langle \mathbf{S}^{\mathrm{T}(j),\mathrm{L}}\bigr\rangle\mathbf{n}\,\mathrm{d}\Omega, \tag{2.8}$$

where $\mathrm{d}\Omega = \sin\theta\,\mathrm{d}\theta\,\mathrm{d}\varphi$ is the solid-angle element. The spectral densities $p^{\mathrm{T}(j),\mathrm{L}}(\omega)$ are obtained by interchanging the $\mathrm{d}\Omega$ and $\mathrm{d}\omega$ integrations, so that $P^{\mathrm{T}(j),\mathrm{L}} = \int p^{\mathrm{T}(j),\mathrm{L}}(\omega)\,\mathrm{d}\omega$. At this stage, the integration over the negative frequency range is converted into an integration over positive frequencies by the variable change $\omega \to -\omega$.

We consider trajectories of type $\mathbf{x}_0(t) = \mathbf{v}t + \boldsymbol{\xi}(t)$, where $\boldsymbol{\xi}(t) = \sum_{k=-\infty}^{+\infty}\boldsymbol{\xi}_k\exp(-\mathrm{i}\tilde{\omega}_k t)$, with $\boldsymbol{\xi}_{-k} = \boldsymbol{\xi}_k^*$ and $\tilde{\omega}_{-k} = -\tilde{\omega}_k$, and $k = 0$ omitted. The constant $\mathbf{v}$ is the uniform speed component, and the frequencies can be arbitrary, not just integer multiples of a base frequency. The series corresponds to a stationary process composed of periodic components with real frequencies $\tilde{\omega}_k$. We will study the ultra-relativistic regime, where multipole expansions of the flux vectors based on the ascending series of $\exp(-\mathrm{i}k(\omega)\mathbf{n}\boldsymbol{\xi}(t))$ break down. In this case, we employ steepest-descent asymptotics resulting in continuous spectral densities, see Sect. 3 and Appendix C. We use the Heaviside–Lorentz system throughout this article, so that $\alpha_\mathrm{e} = e^2/(4\pi\hbar c) \approx 1/137$ and $\alpha_\mathrm{q} = q^2/(4\pi\hbar c) \approx 1.0 \times 10^{-13}$ are the electric and tachyonic fine-structure constants. We here also mention the ratio $\alpha_\mathrm{q}/\alpha_\mathrm{e} \approx 1.4 \times 10^{-11}$ and the tachyon mass $m_\mathrm{t} \approx m/238 \approx 2.15\ \mathrm{keV}/c^2$, inferred from hydrogenic Lamb shifts [5].

More specifically, we will study trajectories in the above parameter representation, and restrict to the first two orders, the first and second harmonics that is,

$$\begin{aligned} \mathbf{x}_0(\varphi) &= \boldsymbol{\xi}_{-1} + \boldsymbol{\xi}_0\varphi + 2\mathrm{Re}\bigl(\boldsymbol{\xi}_1\mathrm{e}^{-\mathrm{i}\tilde{\omega}\varphi}\bigr) \\ &\quad + 2\mathrm{Re}\bigl(\boldsymbol{\xi}_2\mathrm{e}^{-2\mathrm{i}\tilde{\omega}\varphi}\bigr), \\ t(\varphi) &= \tau_{-1} + \tau_0\varphi + 2\mathrm{Re}\bigl(\tau_1\mathrm{e}^{-\mathrm{i}\tilde{\omega}\varphi}\bigr) \\ &\quad + 2\mathrm{Re}\bigl(\tau_2\mathrm{e}^{-2\mathrm{i}\tilde{\omega}\varphi}\bigr), \end{aligned} \tag{2.9}$$

where $\boldsymbol{\xi}_{-1,0}$ are real 3-vectors and $\tau_{-1,0}$ are real constants; the vectors $\boldsymbol{\xi}_{1,2}$ and the constants $\tau_{1,2}$ are complex. At this point, we do not yet decompose the exponentials into trigonometric functions. The first two harmonics suffice to describe all possible trajectories in electromagnetic plane waves, see Appendices A and B. The first harmonic suffices for particles orbiting in constant magnetic fields or circularly polarized plane waves, see (B.14). The Lissajous orbits (B.25) in elliptically polarized waves also depend on the second harmonic in (2.9). The steepest-descent asymptotics employed in Sect. 3 and Appendix C also applies to trajectories defined by higher harmonics, since the spectral densities for curvature radiation in the ultra-relativistic regime are calculated with effective, uniformly curved trajectories obtained by time averaging. The time-averaged orbits of constant curvature (3.1) result in stationary radiation densities (3.11). The averaging procedure (B.16) is worked out in Appendix B for trajectories in electromagnetic plane waves, but can be applied to high-order harmonics in like manner, which arise in more general field configurations such as wave trains obtained by superposition of plane waves as mentioned at the beginning of Appendix A. In the following, we put $\boldsymbol{\xi}_2 = 0$ and $\tau_2 = 0$ in (2.9), as the effective trajectories only depend on the first harmonic, see (3.6).

We first calculate the current transform $\hat{\mathbf{J}}(\mathbf{x}, \omega; T)$ in (2.5) with trajectory (2.9) ($\boldsymbol{\xi}_2 = 0$, $\tau_2 = 0$) substituted. We start by writing the phase in (2.5) as

$$k(\omega)\mathbf{n}\mathbf{x}_0(\varphi) - \omega t(\varphi) = \alpha_{-1} + \alpha_0\varphi + 2\mathrm{Re}\big(\alpha_1 \mathrm{e}^{-\mathrm{i}\tilde{\omega}\varphi}\big), \tag{2.10}$$

$$\begin{aligned} &\alpha_m := k(\omega)\mathbf{n}\boldsymbol{\xi}_m - \omega\tau_m, \\ &\alpha_m(-\omega) = -\alpha_m(\omega), \quad m = -1, 0, 1. \end{aligned} \tag{2.11}$$

We place $\boldsymbol{\xi}_0$ in (2.11) along the z axis, $\boldsymbol{\xi}_0 = \xi_{0,3}\mathbf{e}_3$ (with positive or negative $\xi_{0,3}$), and use the coordinate unit vector $\mathbf{e}_3$ as polar axis, $\mathbf{n}\mathbf{e}_3 = \cos\theta$. We split $\alpha_1 =: \alpha_{1,\mathrm{Re}} + \mathrm{i}\alpha_{1,\mathrm{Im}}$, and define $0 \le \delta < 2\pi$ via $\sin\delta = \alpha_{1,\mathrm{Re}}/|\alpha_1|$ and $\cos\delta = \alpha_{1,\mathrm{Im}}/|\alpha_1|$, to obtain

$$\begin{aligned} &k(\omega)\mathbf{n}\mathbf{x}_0(\varphi) - \omega t(\varphi) \\ &\quad = \alpha_{-1} + \alpha_0\varphi + 2|\alpha_1|\sin(\tilde{\omega}\varphi + \delta). \end{aligned} \tag{2.12}$$

In the current transform (2.5), we substitute the differential

$$\mathrm{d}\mathbf{x}_0(\varphi) = \big(\boldsymbol{\xi}_0 + \mathrm{i}\tilde{\omega}\big(\boldsymbol{\xi}_1^*\mathrm{e}^{\mathrm{i}\tilde{\omega}\varphi} - \boldsymbol{\xi}_1\mathrm{e}^{-\mathrm{i}\tilde{\omega}\varphi}\big)\big)\,\mathrm{d}\varphi, \tag{2.13}$$

and we expand the phase of the integrand in a Fourier series [29],

$$\begin{aligned} &\exp\big(-2\mathrm{i}|\alpha_1|\sin(\tilde{\omega}\varphi + \delta)\big) \\ &\quad = \sum_{n=-\infty}^{+\infty} J_n\big(2|\alpha_1|\big)\exp\big[-\mathrm{i}n(\tilde{\omega}\varphi + \delta)\big]. \end{aligned} \tag{2.14}$$

Here, we may also shift the summation index if convenient, replacing n by $n+1$ or $n-1$ and the resulting Bessel functions $J_{n\pm 1}(z)$ by $J_{n+1} = (n/z)J_n - J_n'$ and $J_{n-1} = (n/z)J_n + J_n'$. The $\mathrm{d}\varphi$ integration (2.13) of the current transform (2.5) is performed by means of the limit definition (2.6) of the Dirac function,

$$\begin{aligned} \hat{\mathbf{J}}(\mathbf{x}, \omega; T) = 2\pi q \mathrm{e}^{-\mathrm{i}\alpha_{-1}} &\sum_{n=-\infty}^{+\infty} \mathrm{e}^{-\mathrm{i}n\delta}\delta_{(1)}(-\alpha_0 - n\tilde{\omega}; T_\varphi) \\ &\times \bigg\{\bigg[\boldsymbol{\xi}_0 + \frac{n\tilde{\omega}}{2|\alpha_1|}\mathrm{i}\big(\boldsymbol{\xi}_1^*\mathrm{e}^{-\mathrm{i}\delta} - \boldsymbol{\xi}_1\mathrm{e}^{\mathrm{i}\delta}\big)\bigg]J_n\big(2|\alpha_1|\big) \\ &\quad - \mathrm{i}\tilde{\omega}\big(\boldsymbol{\xi}_1^*\mathrm{e}^{-\mathrm{i}\delta} + \boldsymbol{\xi}_1\mathrm{e}^{\mathrm{i}\delta}\big)J_n'\big(2|\alpha_1|\big)\bigg\}. \end{aligned} \tag{2.15}$$

We split the amplitude $\boldsymbol{\xi}_1$ into real vectors, $\boldsymbol{\xi}_1 =: \boldsymbol{\xi}_{1,\mathrm{Re}} + \mathrm{i}\boldsymbol{\xi}_{1,\mathrm{Im}}$, and substitute

$$\begin{aligned} &\mathrm{i}\big(\boldsymbol{\xi}_1^*\mathrm{e}^{-\mathrm{i}\delta} - \boldsymbol{\xi}_1\mathrm{e}^{\mathrm{i}\delta}\big) = 2(\boldsymbol{\xi}_{1,\mathrm{Re}}\sin\delta + \boldsymbol{\xi}_{1,\mathrm{Im}}\cos\delta), \\ &\boldsymbol{\xi}_1^*\mathrm{e}^{-\mathrm{i}\delta} + \boldsymbol{\xi}_1\mathrm{e}^{\mathrm{i}\delta} = 2(\boldsymbol{\xi}_{1,\mathrm{Re}}\cos\delta - \boldsymbol{\xi}_{1,\mathrm{Im}}\sin\delta). \end{aligned} \tag{2.16}$$

The polarized squares of the current transform (2.15) occurring in the Poynting vectors (2.7) are calculated via the squared limit definition (2.6) of the Dirac function,

$$\begin{aligned} &\frac{2\pi}{T}\big|\boldsymbol{\varepsilon}_j\hat{\mathbf{J}}(\mathbf{x}, \omega; T)\big|^2 \\ &\quad = \frac{(2\pi q)^2}{|\tau_0|}\sum_{n=-\infty}^{+\infty}\delta_{(2)}\big(-\alpha_0 - n\tilde{\omega}; |T_\varphi|\big) \\ &\qquad \times \big(A^{(j)}(\omega, n)J_n^2\big(2|\alpha_1|\big) + B^{(j)}(\omega)J_n'^2\big(2|\alpha_1|\big)\big), \\ &A^{(j)}(\omega, n) := \bigg[\boldsymbol{\varepsilon}_j\boldsymbol{\xi}_0 + \frac{n\tilde{\omega}}{|\alpha_1|^2}(\boldsymbol{\varepsilon}_j\boldsymbol{\xi}_{1,\mathrm{Re}}\alpha_{1,\mathrm{Re}} \\ &\qquad + \boldsymbol{\varepsilon}_j\boldsymbol{\xi}_{1,\mathrm{Im}}\alpha_{1,\mathrm{Im}})\bigg]^2, \\ &B^{(j)}(\omega) := 4\frac{\tilde{\omega}^2}{|\alpha_1|^2}(\boldsymbol{\varepsilon}_j\boldsymbol{\xi}_{1,\mathrm{Re}}\alpha_{1,\mathrm{Im}} - \boldsymbol{\varepsilon}_j\boldsymbol{\xi}_{1,\mathrm{Im}}\alpha_{1,\mathrm{Re}})^2. \end{aligned} \tag{2.17}$$

In the amplitudes $A^{(j)}(\omega, n)$ and $B^{(j)}(\omega)$, we substitute the polarization vectors $\boldsymbol{\varepsilon}_j$ defined in (C.1). The frequency dependence is via $\alpha_0(\omega)$ and $\alpha_1 = k(\omega)\xi_{1,i}\boldsymbol{\varepsilon}_3\mathbf{e}_i - \omega\tau_1$, where we can use the angular parametrization (C.2). (The tachyonic frequency ω is not to be confused with the angular frequency $\tilde{\omega}$ in the particle trajectory (2.9).)

In the squared current (2.17), we perform the limit $T \to \infty$, which amounts to replacing $\delta_{(2)}$ by the Dirac function $\delta(-\alpha_0 - n\tilde{\omega})$. According to (2.11) and (C.2), $-\alpha_0 - n\tilde{\omega} = \omega\tau_0 - n\tilde{\omega} - k(\omega)\xi_{0,3}\cos\theta$, where $\boldsymbol{\xi}_0 = \xi_{0,3}\mathbf{e}_3$. The ω zeros of the argument $\alpha_0(\omega) + n\tilde{\omega}$ in the delta functions are thus obtained by solving

$$\omega - n\tilde{\omega}/\tau_0 = k(\omega)\upsilon_\parallel\cos\theta, \quad \upsilon_\parallel := \xi_{0,3}/\tau_0. \tag{2.18}$$

We find the zeros of the squared equation as

$$\begin{aligned} &\omega_n^\pm = \frac{n\tilde{\omega}/\tau_0 \pm \upsilon_\parallel\beta_n\cos\theta}{1 - \upsilon_\parallel^2\cos^2\theta}, \\ &\beta_n := \sqrt{n^2\tilde{\omega}^2/\tau_0^2 + m_t^2\big(1 - \upsilon_\parallel^2\cos^2\theta\big)}, \end{aligned} \tag{2.19}$$

with positive $\tilde{\omega}$ and β_n. At large n, only one of the indicated branches solves (2.18), due to the sign in $k(\omega) = \mathrm{sign}(\omega)\sqrt{\omega^2 + m_t^2}$, see (2.3). In fact, using (2.18), we find

$$k\big(\omega_n^\pm\big) = \frac{n(\tilde{\omega}/\tau_0)\upsilon_\parallel\cos\theta \pm \beta_n}{1 - \upsilon_\parallel^2\cos^2\theta}, \tag{2.20}$$

so that $k(\omega_n^+)$ is positive and $k(\omega_n^-)$ negative if defined via (2.18). Thus, ω_n^+ is a solution of (2.18) only if it is positive, and ω_n^- only if negative. (ω_n^+ is positive for sufficiently large positive n, and ω_n^- negative for sufficiently large negative n, provided that τ_0 is positive. If τ_0 is negative, ω_n^- is negative for large positive n. At small n, both or non of the branches $\omega_n^{\pm}$ can be solutions of (2.18).) Finally, we note the identity $k(\omega_n^{\pm}) - \omega_n^{\pm} \upsilon_{\parallel} \cos\theta = \pm\beta_n$, based on (2.19) and (2.20), which is useful when evaluating the delta functions in (2.17),

$$\delta\bigl(-\alpha_0(\omega) - n\tilde{\omega}\bigr) = \frac{1}{|\tau_0|} \sum_{\pm} \frac{1}{\beta_n} \bigl|k(\omega_n^{\pm})\bigr| \theta\bigl(\pm\omega_n^{\pm}\bigr) \delta\bigl(\omega - \omega_n^{\pm}\bigr). \tag{2.21}$$

We substitute the squared current projections (2.17) into the flux vectors (2.7), and perform the frequency integration, which amounts to mere book keeping by virtue of the Dirac functions in (2.21). We find

$$\begin{aligned} \bigl\langle \mathbf{S}^{\mathrm{T}(j)} \bigr\rangle &\sim \frac{(2\pi q)^2 \mathbf{n}}{4(2\pi)^4 r^2} \frac{1}{\tau_0^2} \sum_{n=-\infty}^{+\infty} S_n^{\mathrm{T}(j)}, \\ \bigl\langle \mathbf{S}^{\mathrm{L}} \bigr\rangle &\sim \frac{(2\pi q)^2 \mathbf{n}}{4(2\pi)^4 r^2} \frac{m_{\mathrm{t}}^2}{\tau_0^2} \sum_{n=-\infty}^{+\infty} S_n^{\mathrm{L}}, \end{aligned} \tag{2.22}$$

where the transversal and longitudinal flux coefficients read

$$\begin{aligned} S_n^{\mathrm{T}(j)} &:= \sum_{\pm} \frac{\theta(\pm\omega_n^{\pm})}{\beta_n} \bigl|\omega_n^{\pm}\bigr| \bigl|k\bigl(\omega_n^{\pm}\bigr)\bigr|^2 \\ &\quad \times \bigl[A^{(j)}\bigl(\omega_n^{\pm}, n\bigr) J_n^2\bigl(2\bigl|\alpha_1\bigl(\omega_n^{\pm}\bigr)\bigr|\bigr) \\ &\quad + B^{(j)}\bigl(\omega_n^{\pm}\bigr) J_n'^2\bigl(2\bigl|\alpha_1\bigl(\omega_n^{\pm}\bigr)\bigr|\bigr)\bigr], \\ S_n^{\mathrm{L}} &:= \sum_{\pm} \frac{\theta(\pm\omega_n^{\pm})}{\beta_n} \frac{|k(\omega_n^{\pm})|^2}{|\omega_n^{\pm}|} \\ &\quad \times \bigl[A^{(3)}\bigl(\omega_n^{\pm}, n\bigr) J_n^2\bigl(2\bigl|\alpha_1\bigl(\omega_n^{\pm}\bigr)\bigr|\bigr) \\ &\quad + B^{(3)}\bigl(\omega_n^{\pm}\bigr) J_n'^2\bigl(2\bigl|\alpha_1\bigl(\omega_n^{\pm}\bigr)\bigr|\bigr)\bigr]. \end{aligned} \tag{2.23}$$

At every fixed n, there is a summation over the two roots (2.19), indicated by ± as in (2.21).

The amplitudes $A^{(j)}$ and $B^{(j)}$ are defined in (2.17). We note the symmetries $\omega_n^{\pm} = -\omega_{-n}^{\mp}$, $k(\omega_n^{\pm}) = -k(\omega_{-n}^{\mp})$, and $\alpha_1(\omega_n^{\pm}) = -\alpha_1(\omega_{-n}^{\mp})$, as well as $J_{-n}^2(z) = J_n^2(z)$ and $J_{-n}'^2(z) = J_n'^2(z)$, so that the n summation in (2.22) is symmetric with respect to the substitution $n \to -n$, and we replace it with $2\sum_{n=1}^{\infty}$. For notational convenience, we drop the $n = 0$ term already at this stage, as the bulk of the contribution in the ultra-relativistic limit is at large n. The radiant power (2.8) is found as

$$P^{\mathrm{T}(j)} \sim \sum_{n=1}^{\infty} P_n^{\mathrm{T}(j)}, \qquad P^{\mathrm{L}} \sim \sum_{n=1}^{\infty} P_n^{\mathrm{L}}, \tag{2.24}$$

where the power and flux coefficients are related by a solid-angle integration,

$$\begin{aligned} P_n^{\mathrm{T}(j)} &\sim \frac{q^2}{8\pi^2} \frac{1}{\tau_0^2} \int_0^{2\pi} \int_0^{\pi} S_n^{\mathrm{T}(j)} \sin\theta \, \mathrm{d}\theta \, \mathrm{d}\varphi, \\ P_n^{\mathrm{L}} &\sim \frac{q^2}{8\pi^2} \frac{m_{\mathrm{t}}^2}{\tau_0^2} \int_0^{2\pi} \int_0^{\pi} S_n^{\mathrm{L}} \sin\theta \, \mathrm{d}\theta \, \mathrm{d}\varphi. \end{aligned} \tag{2.25}$$

The angular parametrization of the polarization vectors $\boldsymbol{\varepsilon}_j$ occurring in the amplitude factors $A^{(j)}$ and $B^{(j)}$ of the flux coefficients is defined in (C.2); the same parametrization is used for α_1 in the argument of the Bessel functions.

Further evaluation of the power coefficients requires specifying the trajectory of the radiating charge, that is, the constants in (2.9). In the next section, we derive the tachyonic spectral densities of ultra-relativistic electrons orbiting in plane waves. In this case, the Bessel functions in the flux coefficients (2.23) are replaced by the Nicholson approximation [30]

$$\begin{aligned} J_n^2\bigl(2|\alpha_1|\bigr) &\sim \frac{2^{2/3}}{n^{2/3}} \mathrm{Ai}^2(\lambda), \\ J_n'^2\bigl(2|\alpha_1|\bigr) &\sim \frac{2^{4/3}}{n^{4/3}} \mathrm{Ai}'^2(\lambda), \\ \lambda &:= 2^{1/3} n^{2/3} \biggl(1 - \frac{2}{n} \bigl|\alpha_1\bigl(\omega_n^{\pm}\bigr)\bigr|\biggr), \end{aligned} \tag{2.26}$$

valid for large n and $|\alpha_1|/n = \mathrm{O}(1)$. The angular integration over the squared Airy integrals in the power coefficients (2.25) is done by steepest descent in Sect. 3.

3 Tachyonic curvature radiation of electrons orbiting in polarized plane waves

3.1 Spectral densities of ultra-relativistic electrons in helical orbits

We consider an ultra-relativistic electron in a polarized plane wave, the general setting is explained in Appendix A. To find the spectral densities, we calculate the tachyonic power coefficients (2.25) with the circular helix

$$\begin{aligned} x &= R\cos(\tilde{\omega}\varphi), \qquad y = R\sin(\tilde{\omega}\varphi), \\ z &= \upsilon_{\parallel} \tilde{\beta} \varphi, \qquad t = \tilde{\beta} \varphi, \end{aligned} \tag{3.1}$$

whose parameters are determined by the time averages (B.26) over the wave period. The helical radius, curvature and torsion (denoted by R, κ_{helix} and τ_{helix}, respectively), and the angular frequency $\tilde{\omega}/\tilde{\beta}$ read

$$R := \sqrt{\langle \hat{x}^2\rangle + \langle \hat{y}^2\rangle},$$

$$\tilde{\omega} := \frac{\upsilon_\perp \tilde{\beta}}{R} = \frac{\sqrt{\langle \hat{x}'^2\rangle + \langle \hat{y}'^2\rangle}}{\sqrt{\langle \hat{x}^2\rangle + \langle \hat{y}^2\rangle}}, \qquad \tilde{\beta} := \sqrt{\langle t'^2\rangle}, \tag{3.2}$$

$$\kappa_{\mathrm{helix}} := \frac{1}{R}\frac{\upsilon_\perp^2}{\upsilon_\perp^2 + \upsilon_\parallel^2}, \qquad \tau_{\mathrm{helix}} := \frac{\upsilon_\parallel}{\upsilon_\perp}\kappa_{\mathrm{helix}}.$$

The coordinate averages are explicitly given in (B.26) and at the end of Appendix B. The longitudinal and transversal velocity components $\upsilon_{\parallel,\perp}$ are stated in (B.18), in particular, $\upsilon_\parallel = \sqrt{\langle \hat{z}'^2\rangle}/\tilde{\beta}$. The time-averaged Lorentz factor is

$$\gamma_{\mathrm{av}} = \frac{1}{\sqrt{1 - \upsilon_\parallel^2 - \upsilon_\perp^2}}, \tag{3.3}$$

and the helical pitch angle α_{p} is defined by

$$\upsilon_\perp = \upsilon \sin\alpha_{\mathrm{p}}, \qquad \upsilon_\parallel = \upsilon\cos\alpha_{\mathrm{p}},$$
$$\tan\alpha_{\mathrm{p}} = \frac{\upsilon_\perp}{\upsilon_\parallel} = \frac{\kappa_{\mathrm{helix}}}{\tau_{\mathrm{helix}}}, \tag{3.4}$$

where $\upsilon = \sqrt{\upsilon_\parallel^2 + \upsilon_\perp^2}$ and $0 \le \alpha_{\mathrm{p}} \le \pi$, so that $\kappa_{\mathrm{helix}} = R^{-1}\sin^2\alpha_{\mathrm{p}}$. The overall signs of the space coordinates in (3.1) have been arbitrarily chosen, in particular $\upsilon_\parallel > 0$. [This is tantamount to applying space reflections to the coordinate frame $\hat{\mathbf{e}}_i$ defined in (B.10), which does not affect the spectral densities; the coordinates in (3.1) refer to the normalized triad $\hat{\mathbf{e}}_{0,i}$, see the remarks following (B.11).] By comparing (3.1) to the general trajectory (2.9) (with $\boldsymbol{\xi}_2 = 0$ and $\tau_2 = 0$),

$$\mathbf{x} = \boldsymbol{\xi}_0\varphi + 2\boldsymbol{\xi}_{1,\mathrm{Re}}\cos(\tilde{\omega}\varphi) + 2\boldsymbol{\xi}_{1,\mathrm{Im}}\sin(\tilde{\omega}\varphi),$$
$$t = \tau_0\varphi + 2\tau_{1,\mathrm{Re}}\cos(\tilde{\omega}\varphi) + 2\tau_{1,\mathrm{Im}}\sin(\tilde{\omega}\varphi), \tag{3.5}$$

we can identify

$$\boldsymbol{\xi}_0 = (0, 0, \upsilon_\parallel\tilde{\beta}), \qquad \boldsymbol{\xi}_{1,\mathrm{Re}} = (R/2, 0, 0),$$
$$\boldsymbol{\xi}_{1,\mathrm{Im}} = (0, R/2, 0), \tag{3.6}$$

as well as $\tau_0 = \tilde{\beta}$ and $\tau_1 = 0$.

The angular parametrization of coefficient α_1 in the phase (2.10) reads

$$\alpha_{1,\mathrm{Re}} = \frac{1}{2}k(\omega)R\cos\varphi\sin\theta,$$
$$\alpha_{1,\mathrm{Im}} = \frac{1}{2}k(\omega)R\sin\varphi\sin\theta, \tag{3.7}$$

so that $2|\alpha_1| = kR\sin\theta$, see (2.11) and (C.2). Returning to the frequencies (2.19) and wave numbers (2.20), we consider ω_n^+ for large positive n (since $\tau_0 > 0$), and find

$$\omega_n^+ = \frac{n\tilde{\omega}}{\tilde{\beta}}\frac{1}{1 - \upsilon_\parallel\cos\theta} + \frac{m_{\mathrm{t}}^2}{2}\frac{\tilde{\beta}}{n\tilde{\omega}}\upsilon_\parallel\cos\theta + \mathrm{O}(n^{-2}), \tag{3.8}$$

$$k(\omega_n^+) = \frac{n\tilde{\omega}}{\tilde{\beta}}\frac{1}{1 - \upsilon_\parallel\cos\theta} + \frac{m_{\mathrm{t}}^2}{2}\frac{\tilde{\beta}}{n\tilde{\omega}} + \mathrm{O}(n^{-2}). \tag{3.9}$$

The tachyonic power coefficients (2.25) can be evaluated by steepest descent, the stationary point of $2|\alpha_1|$ being located at $\cos\theta_{\mathrm{c}} \sim \upsilon_\parallel$. Details of the ultra-relativistic asymptotics are given in Appendix C. The power transversally and longitudinally radiated is obtained by summing the power coefficients over the individual modes according to (2.24). We pass to continuous frequencies by identifying $\omega = n\omega_{\mathrm{c}}$, so that the continuous spectral densities read $p^{\mathrm{T}(j),\mathrm{L}}(\omega)\,\mathrm{d}\omega = P_n^{\mathrm{T}(j),\mathrm{L}}\,\mathrm{d}n$, with $n = \omega/\omega_{\mathrm{c}}$. We use the ultra-relativistic power coefficients (C.10), substitute the asymptotic flux coefficients (C.9), and replace the ψ integrations in (C.10) by the respective Airy identities (C.11). The scaling frequency, $\omega_{\mathrm{c}} = \tilde{\omega}/(\tilde{\beta}\sin^2\alpha_{\mathrm{p}})$, is found via the $n \to \infty$ limit of ω_n^+ in (3.8), taken at the stationary phase. In this continuum limit, the spectral variable η in (C.11) reads

$$\eta = \frac{\omega^{2/3}}{\omega_{\mathrm{a}}^{2/3}}\left(1 - \frac{\omega_{\mathrm{b}}^2}{\omega^2}\right)\frac{1}{\gamma_{\mathrm{av}}^2},$$
$$\omega_{\mathrm{a}} := \frac{\tilde{\omega}}{\tilde{\beta}}\sin\alpha_{\mathrm{p}} = \upsilon\kappa_{\mathrm{helix}}, \qquad \omega_{\mathrm{b}} := m_{\mathrm{t}}\gamma_{\mathrm{av}}, \tag{3.10}$$

where κ_{helix} denotes the helical curvature in (3.2) and γ_{av} the Lorentz factor (3.3). We can thus assemble the ultra-relativistic transversal and longitudinal spectral densities as

$$p^{\mathrm{T}(j)}(\omega) = \frac{\alpha_{\mathrm{q}}}{2}\frac{m_{\mathrm{t}}^2\omega}{\omega^2 + m_{\mathrm{t}}^2}\left(1 - \frac{\omega^2}{\omega_{\mathrm{b}}^2}\right)$$
$$\times\left(\int_\eta^\infty \mathrm{Ai}(x)\,\mathrm{d}x + (2 \pm 1)\frac{\mathrm{Ai}'(\eta)}{\eta}\right), \tag{3.11}$$
$$p^{\mathrm{L}}(\omega) = \alpha_{\mathrm{q}}\frac{m_{\mathrm{t}}^2\omega}{\omega^2 + m_{\mathrm{t}}^2}\int_\eta^\infty \mathrm{Ai}(x)\,\mathrm{d}x.$$

These densities also apply in the lower frequency band $\omega \le \omega_{\mathrm{b}}$, where η in (3.10) is negative. ω_{b} is defined in (3.10). α_{q} in (3.11) denotes the tachyonic fine-structure constant, which is not to be confused with the pitch angle α_{p} in (3.4) and (3.10). [We have $\alpha_{\mathrm{q}} = q^2/(4\pi)$ in the Heaviside–Lorentz system; also see the remarks preceding (2.9).] The frequency $\tilde{\omega}$ in the scale factor ω_{a} in (3.10) is the helical angular frequency (3.2). The upper plus sign in $p^{\mathrm{T}(j)}(\omega)$ refers to the $\boldsymbol{\varepsilon}_1$ polarized component $p^{\mathrm{T}(1)}$, the polarization triad being defined in (C.1). The total transversal radiation density $p^{\mathrm{T}}(\omega)$ is found by adding the two linear polarization components, which means to drop ± 1 and the overall factor of $1/2$. The total unpolarized density is thus $p^{\mathrm{T+L}}(\omega) := p^{\mathrm{T}(1)} + p^{\mathrm{T}(2)} + p^{\mathrm{L}}$. We also note the $|\eta| \gg 1$ asymptotics of the Airy integrals [30],

$$\begin{aligned}
\int_{|\eta|}^{\infty} \mathrm{Ai}(x)\,\mathrm{d}x &= \frac{1}{3} - \int_0^{|\eta|} \mathrm{Ai}(x)\,\mathrm{d}x \\
&\sim \frac{1}{2\sqrt{\pi}|\eta|^{3/4}} \exp\left(-\frac{2}{3}|\eta|^{3/2}\right), \\
\int_{-|\eta|}^{\infty} \mathrm{Ai}(x)\,\mathrm{d}x &= \frac{1}{3} + \int_0^{|\eta|} \mathrm{Ai}(-x)\,\mathrm{d}x \\
&\sim 1 - \frac{1}{\sqrt{\pi}|\eta|^{3/4}} \cos\left(\frac{2}{3}|\eta|^{3/2} + \frac{\pi}{4}\right), \\
\mathrm{Ai}'\big(|\eta|\big) &\sim -\frac{|\eta|^{1/4}}{2\sqrt{\pi}} \exp\left(-\frac{2}{3}|\eta|^{3/2}\right), \\
\mathrm{Ai}'\big(-|\eta|\big) &\sim -\frac{|\eta|^{1/4}}{\sqrt{\pi}} \cos\left(\frac{2}{3}|\eta|^{3/2} + \frac{\pi}{4}\right).
\end{aligned} \tag{3.12}$$

In the zero-field limit $|\eta| \to \infty$, the distributions (3.11) converge to the spectral densities (4.18) of a freely moving charge. This residual radiation in the limit of vanishing orbital curvature is discussed in greater detail in Sect. 4.2.

3.2 Spectral and orbital parameters for tachyonic curvature radiation

We summarize the parameters defining helix (3.1) and the spectral variable η in (3.10). It is convenient to rewrite the coordinate averages (B.26) in terms of the dimensionless quantities

$$\hat{a}_{\mathrm{cp}}^2 := \frac{e^2 a_{\mathrm{cp}}^2}{E_0^2|\alpha|}, \qquad \hat{m}^2 := \frac{m^2}{E_0^2|\alpha|}, \tag{3.13}$$

$$\begin{aligned}
P_1 &:= \frac{e^2}{E_0^4\alpha^2}\big((ap)^2 + (bp)^2\big), \\
P_2 &:= \frac{e^4}{E_0^4\alpha^2}\big((a^2-b^2)^2 + 4(ab)^2\big),
\end{aligned} \tag{3.14}$$

where

$$\alpha = \mathrm{sign}(k_3) - \frac{p_3}{E_0}, \qquad a_{\mathrm{cp}}^2 = \frac{a^2+b^2}{2}, \tag{3.15}$$

as defined in (B.2) and (B.20). [The sign of k_3 determines the orientation of the electromagnetic wave vector along the $\mathbf{e}_3$ axis, not to be confused with the helical axis $\hat{\mathbf{e}}_3$ defined in (B.10).] We also introduce the notation, see (B.11) and (B.20),

$$\kappa^2 := \frac{|\hat{\mathbf{e}}_3|^2}{E_0^2} = 1 - |\alpha|\hat{m}^2 + \big(1-|\alpha|\big)\hat{a}_{\mathrm{cp}}^2 + \frac{\hat{a}_{\mathrm{cp}}^4}{4}. \tag{3.16}$$

The $\langle t'^2\rangle$ average in (B.26) can thus be written as

$$\tilde{\beta}^2 := \langle t'^2\rangle = \frac{1}{\alpha^2}\left(1 + \hat{a}_{\mathrm{cp}}^2 + \frac{\hat{a}_{\mathrm{cp}}^4}{4} + \frac{P_1}{2} + \frac{P_2}{32}\right). \tag{3.17}$$

The longitudinal velocity $\upsilon_\parallel$ along the helical axis is

$$\begin{aligned}
\frac{\upsilon_\parallel^2}{c^2} &:= \frac{\langle \hat{z}'^2\rangle}{\tilde{\beta}^2} \\
&= \frac{1}{\alpha^2\tilde{\beta}^2}\left[\kappa^2 + \left(1 + \hat{a}_{\mathrm{cp}}^2 + \frac{\hat{a}_{\mathrm{cp}}^4}{4}\right)\frac{P_1}{2\kappa^2}\right. \\
&\quad \left. + \left(\big(1-|\alpha|\big)^2 + \big(1-|\alpha|\big)\hat{a}_{\mathrm{cp}}^2 + \frac{\hat{a}_{\mathrm{cp}}^4}{4}\right)\frac{P_2}{32\kappa^2}\right],
\end{aligned} \tag{3.18}$$

and the transverse velocity $\upsilon_\perp$ along the helical base circle (defined as in (3.1) with $z=0$) reads

$$\begin{aligned}
\frac{\upsilon_\perp^2}{c^2} &:= \frac{\langle \hat{x}'^2\rangle + \langle \hat{y}'^2\rangle}{\tilde{\beta}^2} \\
&= \frac{1}{|\alpha|\tilde{\beta}^2}\left[\hat{a}_{\mathrm{cp}}^2 - \big(\hat{a}_{\mathrm{cp}}^2 + \hat{m}^2\big)\frac{P_1}{2\kappa^2}\right. \\
&\quad \left. + \big(2 - |\alpha| - \hat{m}^2\big)\frac{P_2}{32\kappa^2}\right].
\end{aligned} \tag{3.19}$$

The helical radius is calculated via (B.26) and the substitutions stated at the end of Appendix B,

$$\begin{aligned}
R^2 &:= \langle \hat{x}^2\rangle + \langle \hat{y}^2\rangle = c^2\tilde{R}^2/\omega_{\mathrm{em}}^2, \\
\tilde{R}^2 &:= \frac{1}{|\alpha|}\left[\hat{a}_{\mathrm{cp}}^2 - \big(\hat{a}_{\mathrm{cp}}^2 + \hat{m}^2\big)\frac{P_1}{2\kappa^2} + \big(2 - |\alpha| - \hat{m}^2\big)\frac{P_2}{128\kappa^2}\right].
\end{aligned} \tag{3.20}$$

Here, we write ω_{em} for the frequency of the electromagnetic plane wave, and we have restored the units; κ, $\tilde{\beta}$, and $\tilde{R}$ are dimensionless quantities. [In Appendices A and B, electromagnetic frequencies are denoted by ω instead of ω_{em} to save notation, as no confusion can arise. In Sects. 2–4, however, ω stands for the frequency of tachyonic radiation modes, for instance, in the spectral densities defined in (3.10) and (3.11), and therefore we label electromagnetic frequencies with a subscript 'em'.]

The initial electronic 4-momentum is parametrized with the injection velocity $\upsilon_{0,i}$ in the usual way, $E_0 = m\gamma_0$ and $p_i = m\gamma_0\upsilon_{0,i}$, where $\gamma_0 = (1-\upsilon_0^2)^{-1/2}$. We use a polar parametrization in momentum space, with the $\mathbf{e}_3$ axis (z axis) as polar axis (parallel or antiparallel to the direction of wave propagation, see Sect. A.2 of Appendix A),

$$\begin{aligned}
&p_1 = p\sin\theta\cos\varphi, \qquad p_2 = p\sin\theta\sin\varphi, \\
&p_3 = p\cos\theta, \qquad p = m\sqrt{\gamma_0^2 - 1},
\end{aligned} \tag{3.21}$$

and parametrize α in (3.15) as

$$\alpha = \mathrm{sign}(k_3) - \frac{\sqrt{\gamma_0^2-1}}{\gamma_0}\cos\theta. \tag{3.22}$$

If the initial 3-momentum is parallel or antiparallel to the electromagnetic wave vector, $\cos\theta = \mathrm{sign}(k_3)$, we find $\gamma_0^2\alpha \to \mathrm{sign}(k_3)/2$ for $\gamma_0 \to \infty$. Thus the product $E_0^2|\alpha|$ in the denominator of the scaled quantities in (3.13) and (3.14) is bounded from below.

The time-averaged Lorentz factor in (3.3) can be written as

$$\gamma_{\mathrm{av}} = \gamma_0 |\alpha| \tilde{\beta}, \tag{3.23}$$

where γ_0 is the initial Lorentz factor E_0/m; this follows from (3.17)–(3.19), (B.27), and (B.28). The ultra-relativistic limit, $\gamma_{\mathrm{av}} \gg 1$, can be realized by $\gamma_0 \gg 1$ and/or $\hat{a}_{\mathrm{cp}} \gg 1$, see (3.17). The spectral variable η in (3.10) depends on the pitch angle α_{p} in (3.4) as well as the helical angular frequency $\tilde{\omega} = \upsilon_\perp \tilde{\beta}/R$ in (3.2), both of which enter into the scale factor ω_{a}. As $\gamma_{\mathrm{av}} \gg 1$ requires $\upsilon \approx 1$ according to (3.3) and (3.4), we can approximate $\sin\alpha_{\mathrm{p}} \approx \upsilon_\perp$, and put $\omega_{\mathrm{a}} = \upsilon_\perp^2/R$ in (3.10). ω_{a} scales linearly with the electromagnetic frequency, $\omega_{\mathrm{a}} \propto \omega_{\mathrm{em}}$.

Remarks

(1) As for the longitudinal velocity $\upsilon_\parallel$, we note that $\upsilon_\parallel \sim 1$ in the limit $\hat{a}_{\mathrm{cp}} \ll 1$ (with $\gamma_0 \gg 1$) as well as in the limit $\hat{a}_{\mathrm{cp}} \gg 1$ (irrespectively of the magnitude of γ_0). Only if $\hat{a}_{\mathrm{cp}} = \mathrm{O}(1)$ (and thus $\gamma_0 \gg 1$ to guarantee $\gamma_{\mathrm{av}} \gg 1$), the velocity components $\upsilon_\parallel$ and $\upsilon_\perp \approx \sin\alpha_{\mathrm{p}}$ can have comparable magnitude. The ultra-relativistic limit, $\gamma_{\mathrm{av}} \gg 1$, is always realized if $\gamma_0 \gg 1$. It is also realized if $\hat{a}_{\mathrm{cp}} \gg 1$, irrespectively of γ_0. (γ_0 does enter in $\hat{a}_{\mathrm{cp}}$, though.) The spectral densities (3.11) only apply in the ultra-relativistic regime, $\gamma_{\mathrm{av}} \gg 1$.

(2) Helix (3.1) refers to the triad $\hat{\mathbf{e}}_{0,i}$ defined after (B.11). This triad can be subjected to space reflections, which do not affect the spectral densities. The electromagnetic wave vector and the initial 3-momentum p_i refer to the coordinate vectors $\mathbf{e}_i$, from which the triad $\hat{\mathbf{e}}_{0,i}$ is obtained by a rotation; the wave propagates along the $\mathbf{e}_3$ axis (z axis), see Sect. A.2 of Appendix A, in particular the derivation of action (A.17).

(3) To compare to tachyonic synchrotron radiation in a constant magnetic field [6] oriented along the z axis, we consider the synchrotron trajectory $x = R\cos(\omega_B t)$, $y = R\sin(\omega_B t)$, $z = \upsilon_\parallel t$, where gyrofrequency, magnetic field, and Lorentz factor are related by $\omega_B = eB/(m\gamma)$. The gyroradius is $R = \upsilon_\perp/\omega_B$, and the velocity components along the base circle and the helical axis are $\upsilon_\perp = \upsilon\sin\theta$ and $\upsilon_\parallel = \upsilon\cos\theta$. The pitch angle α_{p} coincides with the polar angle θ in (3.21), cf. after (B.6), and $\upsilon = \sqrt{\gamma^2 - 1}/\gamma$. In contrast to motion in an electromagnetic plane wave, the Lorentz factor γ and the orbital speed υ coincide with their initial values. The tachyonic synchrotron densities read as in (3.10) and (3.11), with $\omega_{\mathrm{a}} = \omega_B \sin\theta$ and $\gamma_{\mathrm{av}} = \gamma$.

4 Polarized superluminal radiation from ultra-relativistic electrons

We study more quantitatively the tachyonic spectral densities derived in (3.10) and (3.11), considering two different limits. First, we discuss superluminal curvature radiation emitted by electrons orbiting in laser beams, and give numerical estimates assuming ultra-relativistic injection energy and a high-intensity wave field. Figure 1 illustrates the effect of orbital curvature on the radiation density. In Sect. 4.2, we investigate the opposite limit, the residual radiation of ultra-relativistic electrons in the limit of vanishing electromagnetic field strength and orbital curvature. To this end, we consider ultra-relativistic thermal electron populations in active galactic nuclei, and average the radiation densities over the electron distributions. Figures 2–4 show cascade spectra fitted to the TeV spectral maps of two active galactic nuclei. Based on these fits, one can infer the thermodynamic parameters of the electron plasma in the galactic nuclei.

4.1 Transversal and longitudinal tachyons emitted by electrons in ultra-intense laser beams

We discuss the tachyonic spectral densities (3.11) of electrons injected into intense laser fields. The spectral variable η in (3.10) depends on the initial electronic momentum as well as the electromagnetic wave vector, amplitude, and polarization. It is useful to adopt a dimensionless parametrization of the spectral densities. The squared amplitude of the electromagnetic plane wave (A.8) is $2a_{\mathrm{cp}}^2 = a^2 + b^2$, where $a_i = (a_1, a_2, 0)$ and $b_i = (b_1, b_2, 0)$ are electromagnetic polarization vectors defined before (B.20). The time averages of the field strengths, the energy density ρ_{em}, and the energy flux are readily calculated,

$$\langle A_\mu A^\mu \rangle = a_{\mathrm{cp}}^2, \qquad \langle \rho_{\mathrm{em}} \rangle = \langle \mathbf{E}^2 \rangle = \langle \mathbf{B}^2 \rangle = \omega_{\mathrm{em}}^2 a_{\mathrm{cp}}^2, \\ \langle \mathbf{E} \times \mathbf{B} \rangle = \langle \rho_{\mathrm{em}} \rangle \mathbf{k}_0. \tag{4.1}$$

($\omega_{\mathrm{em}}$is the frequency of the plane wave; the subscript has been dropped in Appendices A and B.) We restore the units. In the Heaviside–Lorentz system, $\alpha_{\mathrm{em}} := e^2/(4\pi\hbar c) \approx 1/137$, and $\rho_{\mathrm{em}} = (1/2)(\mathbf{E}^2 + \mathbf{B}^2)$, so that $\langle \rho_{\mathrm{em}} \rangle = \omega_{\mathrm{em}}^2 a_{\mathrm{cp}}^2/c^2$. The dimension of the $\mathbf{E}$ and $\mathbf{B}$ fields is $\sqrt{\mathrm{eV/cm}^3}$, and the electromagnetic flux vector reads $\mathbf{S} = c\mathbf{E} \times \mathbf{B}$. We use orthogonal polarization vectors, placing $a_i = a\mathbf{e}_1$ and $b_i = b\mathbf{e}_2$ along the x and y axes, and scale them in atomic units, $(a, b) = (mc^2/e)(a_0, b_0)$, so that a_0 and b_0 are dimensionless constants. Stokes parameters $s_{0,1}$ are employed instead of a_0 and b_0,

$$s_0 := a_0^2 + b_0^2, \qquad s_1 := a_0^2 - b_0^2, \qquad a_{\mathrm{cp}}^2 = \frac{m^2c^4}{e^2}\frac{s_0}{2}. \tag{4.2}$$

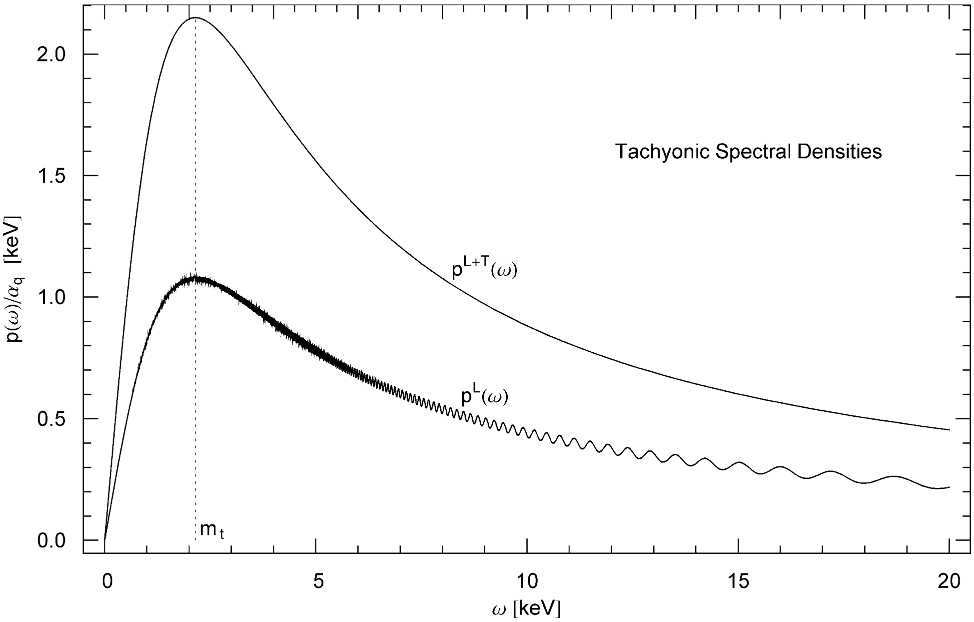

Fig. 1 Superluminal spectral densities of an ultra-relativistic electron orbiting in a linearly polarized electromagnetic plane wave as defined in (3.10) and (3.11). $p^{\rm L+T}$ is the total unpolarized density, $p^{\rm L}$ the longitudinal component, rescaled in the figure with the tachyonic fine-structure constant $\alpha_{\rm q}$. Electromagnetic input parameters: wavelength $\lambda_{\rm em} = 1$ µm, Stokes parameters $s_0 = s_1 = 10^3$ (as defined in (4.2)), intensity $I_{\rm em} \approx 1.37 \times 10^{21}$ W/cm^2. The electronic injection energy is $E_0 = 50$ MeV, with initial momentum antiparallel to the electromagnetic wave vector. The spectral densities are calculated with a time-averaged effective electron trajectory, a helical orbit defined by pitch angle $\sin\alpha_{\rm p} \sim 0.226$, radius $R \approx 1.82 \times 10^{-6}$ cm, gyrofrequency $\omega_{\rm a}/\sin\alpha_{\rm p} \approx 2.45$ eV, and Lorentz factor $\gamma_{\rm av} \approx 99.1$, cf. (4.10)–(4.13). The spectral peak is located at the tachyon mass, $m_{\rm t} \approx 2.15$ keV, followed by an X-ray tail extending to the break frequency (4.10) at $\omega_{\rm b} \approx 213$ keV, where exponential decay sets in (outside the depicted frequency range). The oscillations in the slope of the longitudinal density $p^{\rm L}$ are absent in the unpolarized density $p^{\rm L+T} = p^{\rm L} + p^{\rm T}$, as they are compensated by the oscillations of the transversal radiation component $p^{\rm T}$ (not shown in the figure)

As for the averaged intensity, $\langle I_{\rm em}\rangle = c\langle\rho_{\rm em}\rangle$, we find

$$\langle I_{\rm em}\rangle = \frac{1}{8\pi}\frac{m^2c^2}{\hbar\alpha_{\rm em}}\omega_{\rm em}^2 s_0 = \frac{\pi}{2}\frac{m^2c^4}{\hbar\alpha_{\rm em}}\frac{s_0}{\lambda_{\rm em}^2}, \tag{4.3}$$

$$\begin{aligned}\langle\rho_{\rm em}\rangle[\mathrm{J/cm^3}] &\approx 4.564 \times 10^7 \frac{s_0}{\lambda_{\rm em}^2[\mu\mathrm{m}]}\\ &\approx 2.969 \times 10^{19} s_0 E_{\rm em}^2[\mathrm{MeV}],\end{aligned} \tag{4.4}$$

$$\begin{aligned}\langle I_{\rm em}\rangle[\mathrm{W/cm^2}] &\approx 1.368 \times 10^{18} \frac{s_0}{\lambda_{\rm em}^2[\mu\mathrm{m}]}\\ &\approx 8.900 \times 10^{29} s_0 E_{\rm em}^2[\mathrm{MeV}],\end{aligned} \tag{4.5}$$

where $E_{\rm em}$ is the photon energy $\hbar\omega_{\rm em}$ and $\lambda_{\rm em}$ the (unreduced) wavelength, $\lambda_{\rm em}[\mathrm{cm}] \approx 1.240 \times 10^{-7}/E_{\rm em}[\mathrm{keV}]$, and $\nu_{\rm em}[\mathrm{Hz}] \approx 2.418 \times 10^{17} E_{\rm em}[\mathrm{keV}]$.

We define the averaged field strength as $|\mathbf{E}|_{\rm av} := \sqrt{\langle\mathbf{E}^2\rangle}$ and analogously $|\mathbf{B}|_{\rm av}$, so that $|\mathbf{E}|_{\rm av} = |\mathbf{B}|_{\rm av} = \sqrt{\langle\rho_{\rm em}\rangle}$. By making use of $\sqrt{\mathrm{J/cm}} \approx 9.480 \times 10^5$ V and V/cm $\approx 3.336 \times 10^{-3}$ G, we find, in the Heaviside–Lorentz system,

$$\begin{aligned}|\mathbf{E}|_{\rm av} &\approx 6.404 \times 10^9 \frac{\sqrt{s_0}}{\lambda_{\rm em}[\mu\mathrm{m}]}\frac{\mathrm{V}}{\mathrm{cm}}\\ &\approx 5.166 \times 10^{15}\sqrt{s_0}E_{\rm em}[\mathrm{MeV}]\frac{\mathrm{V}}{\mathrm{cm}},\end{aligned} \tag{4.6}$$

$$\begin{aligned}|\mathbf{B}|_{\rm av} &\approx 2.136 \times 10^7 \frac{\sqrt{s_0}}{\lambda_{\rm em}[\mu\mathrm{m}]}\mathrm{G}\\ &\approx 1.723 \times 10^{13}\sqrt{s_0}E_{\rm em}[\mathrm{MeV}]\mathrm{G}.\end{aligned} \tag{4.7}$$

[As mentioned above and in Sects. 2 and 3, we use the Heaviside–Lorentz system in this article. In the Gaussian system, these field strengths are multiplied by a factor of $\sqrt{4\pi}$, as the fine-structure constant in this system is defined by $e^2/(\hbar c) \approx 1/137$, so that $e|\mathbf{E}|_{\rm av}$, $e|\mathbf{B}|_{\rm av}$, and $e^2a_{\rm cp}^2$ stay invariant. The energy density (4.4) and intensity (4.5) are not affected by this rescaling and thus also apply in the Gaussian system without alterations.] We consider optical and near-infrared wavelengths centered around 1 µm, such as 800 nm for a Ti:sapphire laser, 1064 nm for a Nd:YAG laser (532 nm if frequency-doubled), 248 nm for a KrF laser, and 10.6 µm for a CO$_2$ laser. At these wavelengths, high and ultra-high intensities (in the range 10^{15}–10^{18} W/cm^2 and 10^{18}–10^{21} W/cm^2, respectively [32, 33]) imply amplitudes in the interval $10^{-3} \le s_0 \le 10^3$ according to (4.5), and we note $E_{\rm em}[\mathrm{keV}] \approx 1.240 \times 10^{-3}/\lambda_{\rm em}[\mu\mathrm{m}]$.

The dimensionless coefficients in (3.13) and (3.14) occurring in the spectral variable η are parametrized as

$$\hat{a}_{\mathrm{cp}}^2 = \frac{s_0}{2\gamma_0^2|\alpha|}, \qquad \hat{m}^2 = \frac{1}{\gamma_0^2|\alpha|}, \tag{4.8}$$

$$P_1 = \frac{\gamma_0^2-1}{2\gamma_0^4\alpha^2}\big(s_0 + s_1\cos(2\varphi)\big)\sin^2\theta, \qquad P_2 = \frac{s_1^2}{\gamma_0^4\alpha^2}. \tag{4.9}$$

Here, we use the Stokes parameters (4.2), as well as the polar $(\gamma_0, \theta, \varphi)$ parametrization (3.21) of the initial electronic momentum, and substitute $\alpha(\gamma_0, \theta; \mathrm{sign}(k_3))$ as defined in (3.22). The electromagnetic wave vector is $\mathrm{sign}(k_3)\omega_{\mathrm{em}}\mathbf{e}_3$, the wave propagation being parallel or antiparallel to the z axis according to $\mathrm{sign}(k_3)$. (This convention is also used in the derivation of action (A.17).) The transversal and longitudinal velocity components $\upsilon_{\perp,\parallel}$ and the helical radius R in (3.18)–(3.20) are parametrized by substituting the coefficients (4.8) and (4.9). The scale factor ω_{a} in η is parametrized via $\omega_{\mathrm{a}} = \upsilon_\perp^2/R$, according to (3.10) and the discussion following (3.23). The tachyonic break frequency ω_{b} enters in η and separately in the transversal spectral density in (3.11). ω_{b} and the time-averaged Lorentz factor γ_{av} are parametrized via $\omega_{\mathrm{b}}/m_{\mathrm{t}} = \gamma_{\mathrm{av}} = \gamma_0|\alpha|\tilde{\beta}$, see (3.23), with $\tilde{\beta}$ defined by (3.17), with (4.8) and (4.9) substituted.

To summarize, the spectral variable η in (3.10) is assembled as

$$\eta(\omega) = (\omega/\omega_{\mathrm{a}})^{2/3}\left(1 - \frac{\omega_{\mathrm{b}}^2}{\omega^2}\right)\frac{1}{\gamma_{\mathrm{av}}^2},$$
$$\omega_{\mathrm{a}} = \frac{\upsilon_\perp^2}{c^2}\frac{E_{\mathrm{em}}}{\hbar}\frac{1}{\tilde{R}}, \qquad \omega_{\mathrm{b}} = \frac{m_{\mathrm{t}}c^2}{\hbar}\gamma_{\mathrm{av}}, \qquad \gamma_{\mathrm{av}} = \gamma_0|\alpha|\tilde{\beta}. \tag{4.10}$$

Here, ω is the frequency of the radiated tachyons as it occurs in the spectral densities (3.11), and $E_{\mathrm{em}} = \hbar\omega_{\mathrm{em}}$. The parameters α and $\tilde{\beta}$ are defined in (3.22) and (3.17) respectively,

$$\alpha = \mathrm{sign}(k_3) - \frac{\sqrt{\gamma_0^2-1}}{\gamma_0}\cos\theta,$$
$$\tilde{\beta} = \frac{1}{|\alpha|}\sqrt{1 + \hat{a}_{\mathrm{cp}}^2 + \frac{\hat{a}_{\mathrm{cp}}^4}{4} + \frac{P_1}{2} + \frac{P_2}{32}}, \tag{4.11}$$

where $\mathrm{sign}(k_3)$ indicates the orientation of the electromagnetic wave vector along the z axis. The velocity component $\upsilon_\perp$ along the helical base circle, see (3.19), and the helical radius $R = c\tilde{R}/\omega_{\mathrm{em}}$ in (3.20) are parametrized as

$$\frac{\upsilon_\perp^2}{c^2} = \frac{1}{|\alpha|\tilde{\beta}^2}\left[\hat{a}_{\mathrm{cp}}^2 - (\hat{a}_{\mathrm{cp}}^2 + \hat{m}^2)\frac{P_1}{2\kappa^2} + (2 - |\alpha| - \hat{m}^2)\frac{P_2}{32\kappa^2}\right],$$
$$\tilde{R} = \frac{1}{\sqrt{|\alpha|}}\sqrt{\hat{a}_{\mathrm{cp}}^2 - (\hat{a}_{\mathrm{cp}}^2 + \hat{m}^2)\frac{P_1}{2\kappa^2} + (2 - |\alpha| - \hat{m}^2)\frac{P_2}{128\kappa^2}}, \tag{4.12}$$

where we substitute α and $\tilde{\beta}$ in (4.11), as well as κ^2 introduced in (3.16),

$$\kappa^2 = 1 - |\alpha|\hat{m}^2 + \big(1 - |\alpha|\big)\hat{a}_{\mathrm{cp}}^2 + \hat{a}_{\mathrm{cp}}^4/4. \tag{4.13}$$

It is understood that the quantities $\hat{a}_{\mathrm{cp}}^2$, $\hat{m}^2$, and $P_{1,2}$ occurring in (4.11)–(4.13) are parametrized as in (4.8) and (4.9). The Lamb-shift estimate of the tachyon mass is $m_{\mathrm{t}}c^2 \approx 2.15$ keV [18]. The initial Lorentz factor is related to the injection energy by $\gamma_0 \approx 1957E_0[\mathrm{GeV}]$, and the helical radius to the photon energy $\hbar\omega_{\mathrm{em}}$ by $R[\mathrm{cm}] \approx 1.973 \times 10^{-8}\tilde{R}/E_{\mathrm{em}}[\mathrm{keV}]$.

We briefly enumerate the parameters in the spectral variable $\eta(\omega; \gamma_0, \theta, \varphi; \omega_{\mathrm{em}}, \mathrm{sign}(k_3), s_0, s_1)$ in (4.10). ω is the radiated tachyonic frequency. The parameters $(\gamma_0, \theta, \varphi)$ refer to the injection energy and the initial 3-momentum of the electron, $p_3 = p\cos\theta$, $p = m\sqrt{\gamma_0^2 - 1}$, with polar axis (anti-)parallel to the electromagnetic wave vector $(0, 0, k_3)$, $|k_3| = \omega_{\mathrm{em}}$, see (3.21). The azimuthal φ enters into η only via P_1 in (4.9), and drops out in the case of circular polarization, which means $s_1 = 0$ in (4.2). The remaining four parameters in η determine the electromagnetic plane wave. The frequency ω_{em} enters into the helical radius, $R \propto 1/\omega_{\mathrm{em}}$, according to (3.20) and (4.12). The orientation $\mathrm{sign}(k_3)$ of the wave vector enters in α, see (4.11). Amplitude $\sqrt{s_0}$ and polarization s_1/s_0 enter into η via coefficients (4.8) and (4.9). We also mention that $-1 \le s_1/s_0 \le 1$, and $s_1 = \pm s_0$ holds for linear polarization. The squared amplitude s_0 is determined by intensity I_{em} and frequency ω_{em}, as stated in (4.5). The tachyonic break frequency ω_{b} and the time-averaged electronic Lorentz factor γ_{av} depend on the same set of parameters as η, except for the frequencies ω and ω_{em}, see (4.10).

In Fig. 1, we depict the longitudinal as well as the total unpolarized spectral densities, that is $p^{\mathrm{L}}(\omega)$ and $p^{\mathrm{T+L}}(\omega)$ in (3.11), of an electron colliding head-on with a linearly polarized plane wave. The electron moves along the z axis ($\theta = 0$), antiparallel to the plane wave, $\mathrm{sign}(k_3) = -1$. The electromagnetic wavelength is $\lambda_{\mathrm{em}} = 1$ μm, corresponding to a photon energy of $E_{\mathrm{em}} \approx 1.24$ eV. The Stokes parameters defined in (4.2) are $s_0 = s_1 = 10^3$, which amounts to an intensity of $I_{\mathrm{em}} \approx 1.37 \times 10^{21}$ W/cm^2. The electronic injection energy and the initial Lorentz factor are $E_0 = 50$ MeV and $\gamma_0 \approx 97.9$. These input parameters result in a time-averaged Lorentz factor of $\gamma_{\mathrm{av}} \approx 99.1$ with velocity components $\upsilon_\perp/c \approx 0.226$ and $\upsilon_\parallel/c \approx 0.974$, a helical radius $R \approx 1.82 \times 10^{-6}$ cm, and a pitch angle $\sin\alpha_{\mathrm{p}} \sim \upsilon_\perp/c$. The frequencies defining the spectral variable $\eta(\omega)$ in (4.10) read $\hbar\omega_{\mathrm{a}} \approx 0.552$ eV and $\hbar\omega_{\mathrm{b}} \approx 213$ keV. At this beam intensity, oscillations emerge in the longitudinal and transversal spectral slopes [7, 21], due to the negative mass-square of the radiation.

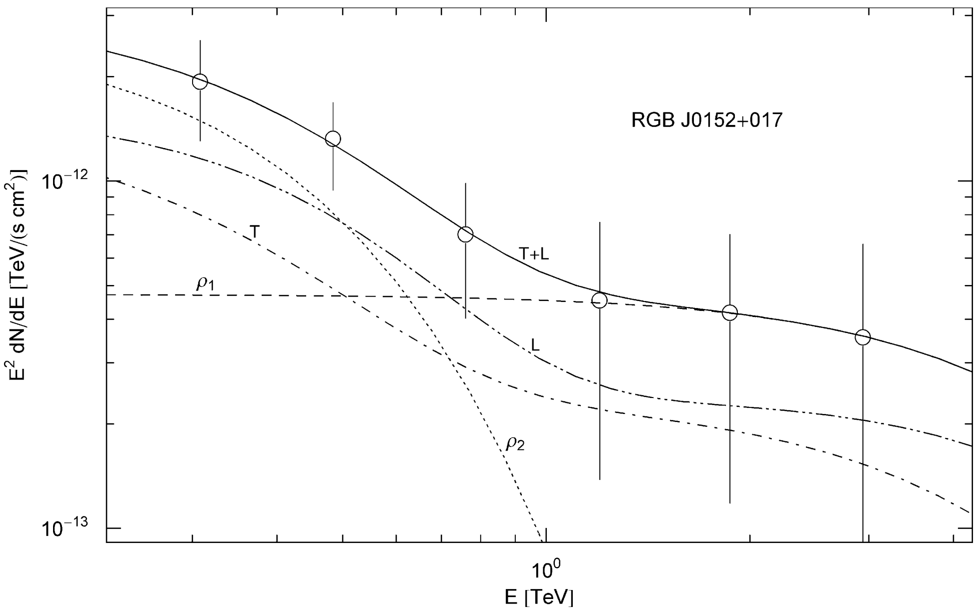

Fig. 2 Spectral map of the BL Lac object RGB J0152 + 017. Data points from Ref. [24]. The solid line T + L depicts the unpolarized differential tachyon flux dN^{T+L}/dE, obtained by adding the flux densities $\rho_{1,2}$ of two thermal ultra-relativistic electron populations, and rescaled with E^2 as in (4.20) for better visibility of the spectral curvature. The transversal (T, *dot-dashed*) and longitudinal (L, *double-dot-dashed*) flux densities $dN^{T,L}/dE$ add up to the total unpolarized flux $T + L = \rho_1 + \rho_2$. The exponential decay of the cascades $\rho_{1,2}$ sets in at about $E_{\rm cut} \approx (m_t/m)kT$, where $m_t/m \approx 1/238$ is the tachyon–electron mass ratio, implying cutoffs at 2.4 TeV for the ρ_1 cascade and 160 GeV for ρ_2. The least-squares fit is performed with the unpolarized tachyon flux T + L, and subsequently split into transversal and longitudinal components. Temperature and source count of the thermal electron plasma generating the cascades are recorded in Table 1

4.2 Tachyonic cascade spectra of ultra-relativistic electron plasmas in active galactic nuclei

The spectral densities (3.11) refer to single charges. We average them with electronic power-law distributions, $d\rho \propto E_0^{-2-\alpha} e^{-E_0/(kT)} d^3p$, where we use the polar $(\gamma_0, \theta, \varphi)$ parametrization (3.21), $d^3p = p^2\, dp \sin\theta\, d\theta\, d\varphi$, with $p = m\sqrt{\gamma_0^2 - 1}$ and $E_0 = m\gamma_0$, to factorize the electron density as

$$d\rho_{\alpha,\beta}(\gamma_0, \theta, \varphi) := \frac{1}{4\pi} \sin\theta\, d\theta\, d\varphi\, d\rho_{\alpha,\beta}(\gamma_0), \tag{4.14}$$

$$\begin{aligned} d\rho_{\alpha,\beta}(\gamma_0) &:= A_{\alpha,\beta}\gamma_0^{-\alpha-1} e^{-\beta\gamma_0} \sqrt{\gamma_0^2 - 1}\, d\gamma_0, \\ &\gamma_1 \le \gamma_0 < \infty, \end{aligned} \tag{4.15}$$

with cutoff exponent $\beta = mc^2/(kT)$ and normalization factor $A_{\alpha,\beta}$. The electronic Lorentz factors range in the interval $\gamma_1 \le \gamma_0 < \infty$, and α is the electronic power-law index. The spectral fits of the active galactic nuclei discussed after (4.19) are performed with ultra-relativistic multi-component plasmas in the collisionless regime [34], with thermal distribution functions defined by $\alpha = -2$ and $\gamma_1 = 1$ in (4.15). The $(\gamma_0, \theta, \varphi)$ parametrization of the tachyonic spectral densities $p^{T(j),L}(\omega; \gamma_0, \theta, \varphi)$ in (3.11) is explained after (4.9); the solid-angle average in (4.14) is carried out as [35]

$$\begin{aligned} &\langle p^{T(j),L}(\omega; \gamma_0)\rangle_\Omega \\ &\quad := \frac{1}{4\pi}\int_0^{2\pi}\int_0^{\pi} p^{T(j),L}(\omega; \gamma_0, \theta, \varphi) \sin\theta\, d\theta\, d\varphi, \end{aligned} \tag{4.16}$$

and the average over the electronic Lorentz factors is performed with density $d\rho_{\alpha,\beta}(\gamma_0)$ in (4.15),

$$\begin{aligned} &\langle p^{T(j),L}(\omega; \gamma_1, n_1)\rangle_{\alpha,\beta} \\ &\quad := \int_{\gamma_1}^{\infty} \langle p^{T(j),L}(\omega; \gamma_0)\rangle_\Omega\, d\rho_{\alpha,\beta}(\gamma_0). \end{aligned} \tag{4.17}$$

In the limit $|\eta| \to \infty$ (that is, for vanishing helical curvature, $\kappa_{\rm helix} \to 0$, at fixed frequency ω, see (3.10)), the spectral densities (3.11) converge to the radiation densities of a uniformly moving charge,

$$\begin{aligned} p^{T,L}(\omega, \gamma) = \frac{\alpha_q m_t^2 \omega}{\omega^2 + m_t^2}\left[\gamma^2 - \left(1 + \frac{\omega^2}{m_t^2}\right)\Delta^{T,L}\right] \\ \times \frac{1}{\gamma\sqrt{\gamma^2 - 1}}, \end{aligned} \tag{4.18}$$

which readily follows from the asymptotic limits of the Airy integrals in (3.12). Here, $\Delta^T = 1$ refers to the transversal radiation, and $\Delta^L = 0$ defines the longitudinal component. In deriving (4.18), we have summed over the two transversal polarization components, $p^T = p^{T(1)} + p^{T(2)}$, and dropped the subscript zero of the electronic Lorentz factor γ. A spectral cutoff occurs at $\omega_{\max}(\gamma) = m_{\rm t}\sqrt{\gamma^2 - 1}$; only frequencies in the range $0 < \omega < \omega_{\max}(\gamma)$ are radiated by a freely moving inertial charge. $\omega_{\max}$ is the counterpart to the break frequency $\omega_{\rm b}$ in (4.10), where the exponential decay of densities (3.11) sets in. The spectral averages (4.16) and (4.17) can be reduced to [36]

$$\begin{aligned} &\langle p^{\rm T,L}(\omega)\rangle_{\alpha,\beta} \\ &\quad = \int_{\gamma_1}^{\infty} p^{\rm T,L}(\omega,\gamma)\theta\big(\omega_{\max}(\gamma) - \omega\big)\, {\rm d}\rho_{\alpha,\beta}(\gamma), \end{aligned} \tag{4.19}$$

with electron density ${\rm d}\rho_{\alpha,\beta}(\gamma)$ in (4.15).

The limit $|\eta| \to \infty$ is realized by vanishing field strength, $a_{\rm cp}^2 \to 0$ or $\omega_{\rm em} \to 0$ according to (4.1), (4.2), and (A.8), so that $\omega_{\rm a} \to 0$ in (4.10). The helical orbits degenerate into inertial motion along straight lines, satisfying the free Hamilton–Jacobi equation (A.1). The fact that inertial particles can emit superluminal radiation is a consequence of the tachyon mass in the Proca Lagrangian (1.1). (In the limit $m_{\rm t} \to 0$, the highest frequency radiated, $\omega_{\max}(\gamma)$, approaches zero.) The residual density (4.18) in the limit of vanishing orbital curvature is due to the negative mass-square of the tachyonic radiation modes, and in strong contrast to electromagnetic radiation processes, which require acceleration.

The most pronounced difference between electromagnetic and tachyonic radiation lies in the emission process itself. Freely moving electrons can radiate superluminal quanta. Radiation densities attached to a uniformly moving charge have no analog in vacuum electrodynamics, their very existence has substantial implications for the spacetime structure, requiring a cosmic absorber medium that breaks the time symmetry of the emission process [37, 38]. The tachyonic radiation densities (4.18) depend on the electronic Lorentz factor in the rest frame of the absorber. The Green function of this radiation process is time symmetric, there is no retarded propagator supported outside the lightcone [39]. The advanced modes of the radiation field are converted into retarded ones by virtue of a nonlocal, instantaneous interaction with the cosmic absorber medium. The latter also defines a universal frame of reference necessary to render the superluminal signal transfer causal. The time symmetry of the Green's function implies that there is no radiation damping, the radiating charge stays in uniform motion. The energy radiated is supplied by the oscillators constituting the absorber medium.

The Wheeler–Feynman absorber theory [37] was motivated by Dirac's covariant version of classical radiation damping [40–42], where the absorber field, half-retarded minus half-advanced, enters as Lorentz force. In Dirac's theory, this field is not perceived as stemming from an absorber medium, but rather as generated by the charge itself; the absorber field does not show as radiation field in the equations of motion, but is exclusively applied along the trajectory of the charge, defining the damping force. In Sect. 2, we have elaborated on superluminal radiation fields at large distance from the source, the opposite limit, as the asymptotic fields suffice to calculate the spectral densities. It is better not to rely on the short distance behavior of Green functions, since the self-energy problem indicates that Maxwell's theory may just be the asymptotic limit of a nonlinear Born−Infeld type of electrodynamics [43]. If so, it is not advisable to use the linearized theory in the vicinity of the radiating sources. The same holds for the Proca field (1.1).

Wheeler and Feynman designed the absorber theory for electrodynamics, and they interpreted the half-retarded minus half-advanced Liénard–Wiechert potential as generated by an absorber medium, which they proposed to be the collection of electric charges in the universe [37]. They used this potential in an action-at-a-distance electrodynamics [38], in an attempt to solve the radiation damping problem. In the Maxwell theory, an absorber field is not necessary, as there is a retarded Green function. Outside the lightcone, however, retardation can only be achieved by an absorber field [39], as the Green's function supported there is time symmetric.

In the spectral fits of the galactic nuclei in Figs. 2–4, electromagnetic emission processes and radiation damping need not be considered, as the radiation is generated by uniformly moving charges, and inertial particles cannot emit photons. Additional electromagnetic or hadronic radiation mechanisms resulting in photonic TeV γ-rays are possible, but this needs further assumptions, such as a proton distribution giving rise to proton-proton scattering followed by pion decay, or a seed photon distribution for inverse Compton scattering. In any case, the tachyonic cascade fits discussed below require fewer input parameters than electromagnetic or hadronic processes, namely temperature and number count of the ultra-relativistic electron plasma, see the caption of Table 1. As the observed spectra are quite efficiently fitted with tachyonic cascades, it is not necessary to assume admixtures of electromagnetic or hadronic radiation processes.

The spectral fits are performed with the classical radiation density (4.18). Its quantized counterpart [7, 17] only differs by terms depending on the tachyon-electron mass ratio, which are too small to noticeably affect the fits, see the caption to Fig. 2. The spectral densities (3.11) and their limit (4.18) for vanishing electromagnetic field strength are classical. Quantum corrections can be calculated by assembling the current (matrix) defining the flux vectors in Sect. 2 with the eigenmodes of the Dirac equation in the electromagnetic plane wave [44].

Figure 2 shows the tachyonic spectral map of the TeV blazar RGB J0152 + 017, at a redshift of $z \approx 0.080$ [24, 45], which translates into a distance of 350 Mpc via $d[\mathrm{Mpc}] \approx$

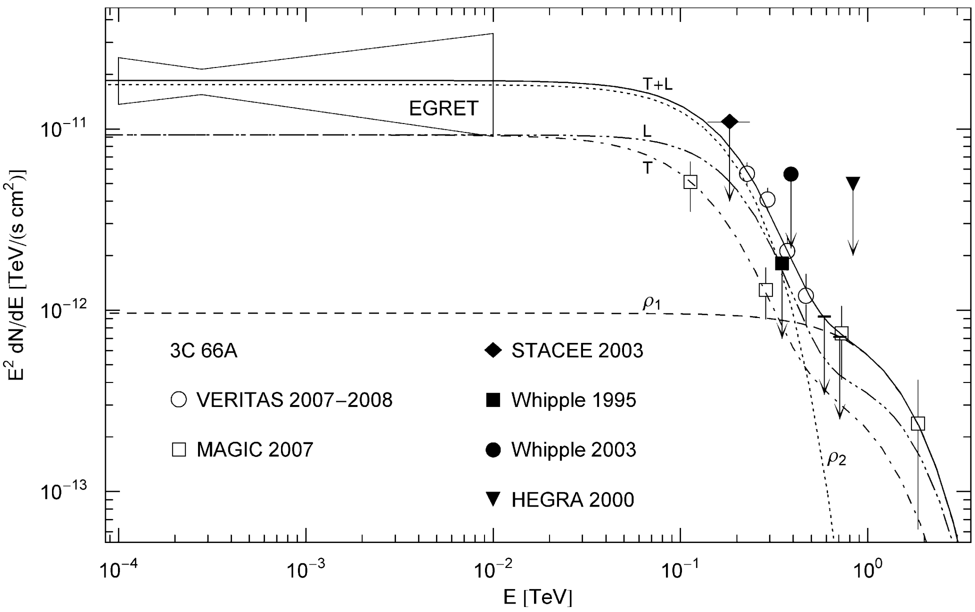

Fig. 3 γ-Ray wideband of the blazar 3C 66A. Notation as in Fig. 2. VERITAS flux points from Ref. [25], MAGIC data points refer to the TeV source MAGIC J0223 + 430 [26]. Upper flux limits from STACEE [47], Whipple [48], and HEGRA [49]. The EGRET bow-tie [47] refers to the associated γ-ray source 3EG J0222 + 4253. The unpolarized tachyon flux $\mathrm{T}+\mathrm{L}=\rho_1+\rho_2$ is generated by a two-component electron plasma, see Table 1. The cutoff energies are 550 GeV for the ρ_1 cascade and 72 GeV for ρ_2. The spectral plateau in the MeV–GeV range is also visible in the preliminary Fermi-LAT data [45]

$4.4\times 10^3 z$ ($h_0\approx 0.68$). The cascades are plots of the E^2-rescaled flux densities

$$E^2\frac{\mathrm{d}N^{\mathrm{T,L}}}{\mathrm{d}E}=\frac{\omega}{4\pi d^2}\langle p^{\mathrm{T,L}}(\omega)\rangle_{\alpha,\beta}, \tag{4.20}$$

where d is the distance to the source, and $\langle p^{\mathrm{T,L}}(\omega=E/\hbar)\rangle$ the averaged transversal/longitudinal spectral density (4.19). The least-squares fit is performed with the unpolarized flux density $\mathrm{d}N^{\mathrm{T+L}}=\mathrm{d}N^{\mathrm{T}}+\mathrm{d}N^{\mathrm{L}}$. The details of the spectral fitting have been explained in [35], and the parameters of the electron distribution $\mathrm{d}\rho_{\alpha,\beta}$ are listed in Table 1. The electronic source number is calculated via

$$n^{\mathrm{e}}\approx 5.75\times 10^{55}\hat{n}d^2[\mathrm{Mpc}], \tag{4.21}$$

where $\hat{n}$ is the tachyonic flux amplitude extracted from the χ^2 fit. TeV γ-ray spectra of active galactic nuclei are usually assumed to be generated by inverse Compton scattering or proton-proton scattering. Both mechanisms result in a flux of high-energy photons partially absorbed by interaction with the infrared background radiation. By contrast, the extragalactic tachyon flux is not attenuated by interaction with the background light. The spectral curvature apparent in double-logarithmic plots of the E^2-rescaled flux densities (4.20) is intrinsic, caused by the Boltzmann factor of the electron distributions (4.15) generating the tachyon flux [28, 46].

The tachyonic cascade fit of the BL Lac object 3C 66A [25, 26, 47–49] is shown in Figs. 3 and 4. The redshift $z\approx 0.444$ of 3C 66A implies a distance of 1.95 Gpc, and the electron number n^{e} of the source plasma is estimated by means of (4.21). The cutoff parameter of the thermal cascades is related to the electron temperature by $kT\,[\mathrm{TeV}]\approx 5.11\times 10^{-7}/\beta$, and the internal energy of the electron populations in Table 1 is based on $U[\mathrm{erg}]\sim 2.46\times 10^{-6}n^{\mathrm{e}}/\beta$ [36], which is the high-temperature limit of the internal energy of a thermal ($\alpha=-2, \gamma_1=1$) ultra-relativistic source distribution (4.15). As mentioned above, there is no absorption of tachyonic γ-rays, since tachyons cannot interact with photons. We may compare Fig. 4 to the spectral maps of the BL Lac objects W Comae ($z\approx 0.102$, 450 Mpc), 1ES 2344+514 ($z\approx 0.044$, 190 Mpc), and PG 1553 + 113 ($z\approx 0.36$, 1.6 Gpc) in [46], as well as to the cascade spectra of H2356 − 309 ($z\approx 0.165$, 730 Mpc), 1ES 1218 + 304 ($z\approx 0.182$, 800 Mpc) and 1ES 1101 − 232 ($z\approx 0.186$, 820 Mpc) in [20], and of the Markarian galaxy Mkn 421 ($z\approx 0.031$, 140 Mpc) in [50]. The curvature in the spectral slopes of these BL Lacs is more pronounced than of the blazar 3C 66A, even though they have a lower redshift. That is, if the curvature were generated by intergalactic absorption, the spectral slopes of the more distant sources should be more strongly curved than that of 3C 66A, but one arrives at the opposite result when comparing the quoted spectral maps with 3C 66A in Figs. 3 and 4. This leads to the conclusion that the curvature in the γ-ray spectra of TeV blazars is uncorrelated with distance. The curvature of the cascades depicted in Figs. 2–4 is generated by the Boltzmann factor of the electron plasma in the galactic nuclei. One may also compare with the Galactic γ-ray binary LS 5039, whose spectral map [36] is more strongly curved than of the galactic nucleus 3C 66A.

We have studied here TeV spectra. Tachyonic spectral fitting in the soft γ-ray band is discussed in [23, 51], where we fit γ-ray burst spectra generated by nonlocal plasma currents.

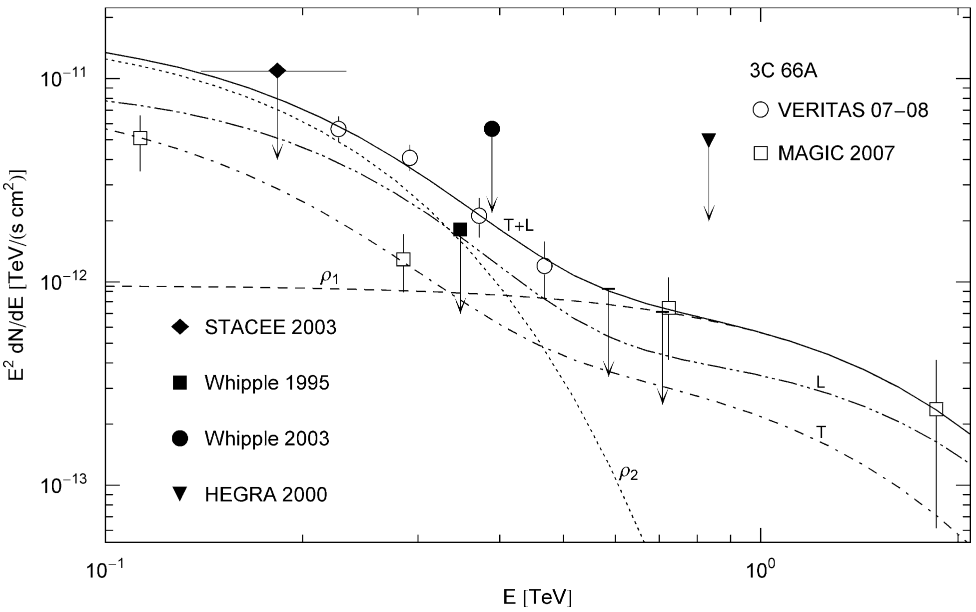

Fig. 4 Close-up of the high-energy spectral slope of the BL Lac object 3C 66A in Fig. 3. T and L stand for the transversal and longitudinal flux components, and T + L labels the unpolarized flux. The first two MAGIC points have not been included in the χ^2 fit, but turn out to be located on the transversal flux component, suggesting the γ-ray source MAGIC J0223 + 430 to be associated with blazar 3C 66A. The curvature of the spectral slope is comparable to that of RGB J0152 + 017 in Fig. 2 at a much lower redshift, see Table 1. The spectral curvature of the rescaled flux density $E^2\,\mathrm{d}N^{\mathrm{T+L}}/\mathrm{d}E$ is uncorrelated with redshift, and generated by the Boltzmann factor of the thermal electronic source plasma in the galactic nucleus

Table 1 Electronic source distributions ρ_i generating the tachyonic cascade spectra of the BL Lac objects RGB J0152 + 017 and 3C 66A in Figs. 2–4. Each ρ_i stands for a thermal ultra-relativistic Maxwell–Boltzmann density (defined by $\alpha = -2$ and $\gamma_1 = 1$ in (4.15)) with cutoff parameter β in the Boltzmann factor. $\hat{n}$ determines the amplitude of the tachyon flux as well as the normalization of the electron density ρ_i, from which the electron count n^{e} is inferred at the indicated distance d, cf. (4.21). kT is the temperature and U the internal energy of the thermal electron plasma. The tachyonic γ-ray cascades labeled $\rho_{1,2}$ in the figures are produced by the corresponding electronic source distributions in this table; each cascade depends on two fitting parameters β and $\hat{n}$ extracted from the χ^2 fit T + L depicted in the figures

	β	$\hat{n}$	d	n^{e}	kT (TeV)	U (erg)
RGB J0152 + 017			$z \approx 0.080$			
ρ_1	8.96×10^{-10}	5.1×10^{-5}	350 Mpc	3.6×10^{56}	570	9.9×10^{59}
ρ_2	1.34×10^{-8}	2.9×10^{-4}		2.1×10^{57}	38	3.8×10^{59}
3C 66A			$z \approx 0.444$			
ρ_1	3.91×10^{-9}	1.0×10^{-4}	1.95 Gpc	2.2×10^{58}	130	1.4×10^{61}
ρ_2	2.99×10^{-8}	1.9×10^{-3}		4.2×10^{59}	17	3.4×10^{61}

5 Conclusion

We derived the tachyonic spectral densities of electrons accelerated in ultra-intense laser fields, and discussed their dependence on the beam intensity, wavelength, and polarization. The acceleration of the radiating electron is manifested in modulations along the power-law slopes of the transversal and longitudinal radiation components, see Fig. 1. The polarization of tachyons can be determined from the transversal and longitudinal ionization cross-sections of Rydberg atoms, which peak at different scattering angles [52]. We considered ultra-relativistic electron orbits, resulting in continuous spectral densities. Non-relativistic motion in plane waves gives rise to discrete, cyclotron-like spectra [53]. In this case, one has to use the exact orbits instead of their time averages when calculating the tachyonic power coefficients, and a multipole expansion of the superluminal flux vectors instead of the steepest-descent asymptotics employed in Sect. 3 and Appendix C to derive the continuous spectral densities.

In Figs. 2–4, we fitted the spectral maps of TeV blazars with tachyonic cascade spectra, and resolved the transversal and longitudinal polarization components. The spectral curvature as well as the spectral plateau in the MeV–GeV range, which emerges in the rescaled logarithmic flux representation used in the figures, can be fitted with superluminal γ-ray cascades generated by thermal electron populations in the active galactic nucleus. Traditional radiation mechanisms such as inverse Compton scattering fail to reproduce extended spectral plateaus, a fact often concealed by compression in broadband maps. We showed that absorption of electromagnetic radiation due to interaction with background photons is not a viable explanation of spectral curvature, since the curvature would increase with distance if affected by intergalactic absorption. This is not the case as pointed out in Sect. 4.2 and the caption to Fig. 4, whereas tachyonic γ-rays propagate unattenuated over intergalactic distances. The curvature of the cascade spectra is intrinsic, generated by the Boltzmann factor of the electronic source plasma.

Acknowledgements The author acknowledges the support of the Japan Society for the Promotion of Science. The hospitality and stimulating atmosphere of the Centre for Nonlinear Dynamics, Bharathidasan University, Trichy, and the Institute of Mathematical Sciences, Chennai, are likewise gratefully acknowledged. I also thank the referees for a careful reading and useful suggestions to improve the manuscript.

Appendix A: Ultra-relativistic charges in wave pulses and plane waves

A.1 Fourier decomposition of the action functional

We start with the Hamilton–Jacobi equation for a charge e in an electromagnetic wave,

$$\eta^{\mu\nu}(S_{,\mu}-eA_\mu)(S_{,\nu}-eA_\nu)+m^2=0, \tag{A.1}$$

where the sign convention is $\eta_{\mu\nu}=\mathrm{diag}(-1,1,1,1)$. With regard to energy, the convention is $p_\mu=(-E,\mathbf{p})$ for particles and $k_\mu=(-\omega,\mathbf{k})$ for photons, with $E>0$ and $\omega=|\mathbf{k}|$. In the case of a free particle, these sign conventions are such that the action reads $S=p_\mu x^\mu=-Et+\mathbf{px}$, with $E=\sqrt{p^2+m^2}$, $p=|\mathbf{p}|$, and $p_\mu p^\mu=-m^2$.

We consider an electromagnetic pulse composed of plane waves with wave vectors aligned in the same direction. That is, we attach to every frequency ω_n a wave vector $k_{\mu,n}:=\omega_n\hat{k}_\mu$, with $\hat{k}_\mu:=(-1,\mathbf{k}_0)$, where $\mathbf{k}_0$ is an arbitrary real unit vector, the same for all modes. We define $\varphi:=-\hat{k}_\mu x^\mu=t-\mathbf{k}_0\mathbf{x}$, so that $k_{\mu,n}x^\mu=-\omega_n\varphi$, and consider the wave train $A_\mu=\sum\tilde{A}_{\mu,n}\exp(-\mathrm{i}\omega_n\varphi)+\text{c.c.}$, where the amplitudes satisfy the Lorentz condition $\tilde{A}_{\mu,n}\hat{k}^\mu=0$. Otherwise, the $\tilde{A}_{\mu,n}$ are arbitrary constant complex 4-vectors. The frequencies ω_n are positive, typically multiples $\omega_n=n\omega$ of a base frequency ω, but it is convenient to formally extend the summation to include negative frequencies, defining $\omega_{-n}=-\omega_n$ and $\tilde{A}_{\mu,-n}=\tilde{A}^*_{\mu,n}$, as well as $\tilde{A}_{\mu,0}=0$, and $\omega_0=0$, so that $A_\mu(\varphi)=\sum_{n=-\infty}^{+\infty}\tilde{A}_{\mu,n}\exp(-\mathrm{i}\omega_n\varphi)$. This wave field satisfies the Lorentz condition $A_\mu\hat{k}^\mu=0$. We may put $A_0=0$ via a gauge transformation, $A_\mu\to A_\mu-\partial_\mu\chi$, with $\chi(\varphi)=\int A_0(\varphi)\,\mathrm{d}\varphi$, but we do not assume this at this stage. To solve (A.1), we use the ansatz [44, 54–56]

$$S=p_\mu x^\mu+\int f(\varphi)\,\mathrm{d}\varphi, \tag{A.2}$$

so that $S_{,\mu}=p_\mu-f(\varphi)\hat{k}_\mu$, and obtain

$$f(\varphi)=-\frac{1}{2\hat{k}_\mu p^\mu}\left(2eA^\mu p_\mu-e^2A_\mu A^\mu-p_\mu p^\mu-m^2\right). \tag{A.3}$$

We put $p^2=-m^2$ and drop the last two terms in (A.3). [Indices in scalar products of 4-vectors will usually not be indicated. For instance, we write kp for $k_\mu p^\mu:=-k_0p_0+k_mp^m$, where $k_\mu=(k_0,k_m)$ and $p_\mu=(p_0,p_m)$; the sign convention for the Minkowski metric is thus $\eta_{\mu\nu}=\mathrm{diag}(-1,1,1,1)$. Greek indices are used for 4-vectors, Latin ones for 3-vectors.] In fact, if this relation does not hold, we may replace p_μ in S by $p'_\mu:=p_\mu-\kappa\hat{k}_\mu$ without altering the value of S, where κ is an arbitrary constant. To obtain $p'^2=-m^2$, we choose $\kappa=(p^2+m^2)/(2\hat{k}p)$. Hence,

$$f(\varphi)=-\frac{1}{\hat{k}_\mu p^\mu}\left[e\sum_n\tilde{a}_n\exp(-\mathrm{i}\omega_n\varphi)-\frac{e^2}{2}\sum_{\substack{m,n\\ m+n\neq0}}\tilde{b}_{mn}\exp(-\mathrm{i}\omega_{mn}\varphi)-\frac{e^2}{2}\tilde{b}_0\right], \tag{A.4}$$

where n and m run over all integers, and we introduce the notation $\omega_{mn}:=\omega_m+\omega_n$ and

$$\tilde{a}_n:=\tilde{A}_{\mu,n}p^\mu,\qquad \tilde{b}_{mn}:=\tilde{A}_{\mu,m}\tilde{A}^\mu_{,n},\qquad \tilde{b}_0:=\sum_n\tilde{A}_{\mu,-n}\tilde{A}^\mu_{,n}. \tag{A.5}$$

The action thus reads

$$S=S_0+\hat{S}(\varphi),\qquad S_0:=p_\mu x^\mu+\frac{e^2\tilde{b}_0\varphi}{2\hat{k}_\mu p^\mu},\qquad \hat{S}(\varphi):=\int f(\varphi)\,\mathrm{d}\varphi-\frac{e^2\tilde{b}_0\varphi}{2\hat{k}_\mu p^\mu}, \tag{A.6}$$

where we substitute $f(\varphi)$ to find

$$\hat{S}(\varphi)=\frac{1}{\hat{k}_\mu p^\mu}\left[e\sum_n\frac{\tilde{a}_n}{\mathrm{i}\omega_n}\exp(-\mathrm{i}\omega_n\varphi)-\frac{e^2}{2}\sum_{\substack{m,n\\ m+n\neq0}}\frac{\tilde{b}_{mn}}{\mathrm{i}\omega_{mn}}\exp(-\mathrm{i}\omega_{mn}\varphi)\right]. \tag{A.7}$$

This is the action in a general wave pulse; in the following, we restrict to a single mode.

A.2 Lorentz factor and kinetic momentum

We consider the plane wave

$$\begin{aligned} A_\mu &= \tilde{A}_\mu \exp(-\mathrm{i}\omega\varphi) + \text{c.c.} \\ &= a_\mu \cos(\omega\varphi) - b_\mu \sin(\omega\varphi), \end{aligned} \tag{A.8}$$

$$\begin{aligned} A_\mu A^\mu &= \frac{1}{2}\big(a^2 - b^2\big)\cos(2\omega\varphi) - ab\sin(2\omega\varphi) \\ &\quad + \frac{1}{2}\big(a^2 + b^2\big), \end{aligned} \tag{A.9}$$

where $\tilde{A}_\mu = (a_\mu - \mathrm{i}b_\mu)/2$, with two constant real vectors a_μ and b_μ, subject to $a_\mu k^\mu = b_\mu k^\mu = 0$. We note $\varphi = -\hat{k}_\mu x^\mu = t - \mathbf{k}_0\mathbf{x}$, $\hat{k}_\mu = (-1, \mathbf{k}_0)$, $|\mathbf{k}_0| = 1$, and $k_\mu := \omega\hat{k}_\mu$, as defined after (A.1). The action (A.6) reduces to

$$S = S_0 + \hat{S}(\varphi), \qquad S_0 := p_\mu x^\mu + e^2\frac{\tilde{A}_\mu \tilde{A}^{*\mu}}{\hat{k}_\mu p^\mu}\varphi, \tag{A.10}$$

$$\begin{aligned} \hat{S}(\varphi) := \frac{1}{\mathrm{i}\omega\hat{k}_\mu p^\mu}\bigg[& e\big(\tilde{A}_\mu p^\mu \exp(-\mathrm{i}\omega\varphi) - \text{c.c.}\big) \\ & - \frac{e^2}{4}\big(\tilde{A}_\mu \tilde{A}^\mu \exp(-2\mathrm{i}\omega\varphi) - \text{c.c.}\big)\bigg], \end{aligned} \tag{A.11}$$

and the integrand in (A.2) reads

$$f(\varphi) = \hat{S}'(\varphi) + e^2\frac{\tilde{A}_\mu \tilde{A}^{*\mu}}{\hat{k}_\mu p^\mu}. \tag{A.12}$$

If we refrain from complex notation, we find

$$S_0 = p_\mu x^\mu + e^2(A_2 + B_2)\omega\varphi, \tag{A.13}$$

$$\begin{aligned} \hat{S}(\varphi) &= -e\big(A_1 \sin(\omega\varphi) + B_1 \cos(\omega\varphi)\big) \\ &\quad + \frac{e^2}{2}\big((A_2 - B_2)\sin(2\omega\varphi) + C_2\cos(2\omega\varphi)\big), \end{aligned} \tag{A.14}$$

$$f(\varphi) = \hat{S}'(\varphi) + e^2(A_2 + B_2)\omega, \tag{A.15}$$

with coefficients

$$\begin{aligned} & A_1 = \frac{a_\mu p^\mu}{\omega\hat{k}_\mu p^\mu}, \qquad B_1 = \frac{b_\mu p^\mu}{\omega\hat{k}_\mu p^\mu}, \qquad A_2 = \frac{a_\mu a^\mu}{4\omega\hat{k}_\mu p^\mu}, \\ & B_2 = \frac{b_\mu b^\mu}{4\omega\hat{k}_\mu p^\mu}, \qquad C_2 = \frac{a_\mu b^\mu}{2\omega\hat{k}_\mu p^\mu}. \end{aligned} \tag{A.16}$$

The action $S = S_0 + \hat{S}(\varphi)$ simplifies if $A_\mu A^\mu$ is constant, as it happens for circular polarization implying $a^2 = b^2$ and $ab = 0$.

Furthermore, $ap := a_0 E_0 + a_i p^i$, with $E_0 = -p_0 = \sqrt{p_i^2 + m^2}$. The action is parametrized with the initial free 3-momentum p_i, via the substitution $p_0(p_i)$ in the vector products ap, bp, and $\hat{k}_\mu p^\mu$, which determine the coefficients A_k, B_k, and C_2 in (A.16). Differentiation with respect to p_i is indicated by a subscript preceded by a comma, e.g. $(ap)_{,i} = a_0 p_i/E_0 + a_i$. As the coefficients A_k, B_k, and C_2 enter linearly in $\hat{S}(\varphi)$, we obtain the p_i derivatives $\hat{S}_{,i}(\varphi)$ just by replacing these coefficients by $A_{k,i}$, $B_{k,i}$, and $C_{2,i}$, respectively. We will list the latter derivatives in (A.27) and (A.28), after having specified the polarization vectors a_μ and b_μ.

We place the wave vector $k_\mu = \omega\hat{k}_\mu$ along the z axis, $\mathbf{k}_0 = (0, 0, \operatorname{sign}(k_3))$, $|k_3| = \omega$. On substituting $z = \operatorname{sign}(k_3)(t - \varphi)$ into S_0 defined in (A.13), we find

$$\begin{aligned} S &= \big(\operatorname{sign}(k_3)p_3 - E_0\big)t + p_1 x + p_2 y \\ &\quad - \big[\operatorname{sign}(k_3)p_3 - e^2(A_2 + B_2)\omega\big]\varphi + \hat{S}(\varphi), \end{aligned} \tag{A.17}$$

with $\hat{S}(\varphi)$ in (A.14). The x and y coordinates of the trajectories are obtained by p_i differentiation,

$$S_{,i} = x^i - \frac{p_i}{E_0}t + e^2(A_{2,i} + B_{2,i})\omega\varphi + \hat{S}_{,i}(\varphi) = c_i, \tag{A.18}$$

with $i = 1, 2$. The c_i are integration constants. The φ parametrization of time is found by solving

$$\begin{aligned} & S_{,3} = \alpha t - \big[\operatorname{sign}(k_3) - e^2(A_{2,3} + B_{2,3})\omega\big]\varphi + \hat{S}_{,3}(\varphi) = c_3, \\ & \alpha := \operatorname{sign}(k_3) - \frac{p_3}{E_0} = \frac{p_0 + p_3\operatorname{sign}(k_3)}{p_0\operatorname{sign}(k_3)}. \end{aligned} \tag{A.19}$$

$t(\varphi)$ is substituted into (A.18) to obtain the x and y coordinates in φ parametrization, and the z coordinate is found as $z = \operatorname{sign}(k_3)(t(\varphi) - \varphi)$.

The φ parametrized velocity reads

$$\begin{aligned} & \upsilon_i = x'^i(\varphi)/t'(\varphi), \qquad \upsilon_3 = z'(\varphi)/t'(\varphi), \\ & x'^i(\varphi) = -\frac{p_i}{p_0}t'(\varphi) - f_{,i}(\varphi), \\ & z'(\varphi) = -\frac{p_3 + p_0 f_{,3}(\varphi)}{p_0 + p_3\operatorname{sign}(k_3)}, \\ & t'(\varphi) = p_0\frac{1 - \operatorname{sign}(k_3)f_{,3}(\varphi)}{p_0 + p_3\operatorname{sign}(k_3)}, \end{aligned} \tag{A.20}$$

where we used (A.15). Subscript commas indicate differentiation with respect to p_i. We eliminate the p_i derivatives in (A.20) by differentiation of the Hamilton–Jacobi equation, see (A.1)–(A.3),

$$\begin{aligned} m^2 &= (p_0 - eA_0 + f)^2 - (p_i - eA_i)^2 \\ &\quad - \big(p_3 - eA_3 - \operatorname{sign}(k_3)f\big)^2, \end{aligned} \tag{A.21}$$

where $p^2 = -m^2$ and $A_\mu\hat{k}^\mu = 0$. Hence,

$$\begin{aligned} x'^i &= -\frac{1}{\hat{k}p}(p_i - eA_i), \\ z' &= -\frac{1}{\hat{k}p}\big(p_3 - eA_3 - \mathrm{sign}(k_3) f\big), \\ t' &= \frac{1}{\hat{k}p}(p_0 - eA_0 + f), \\ \hat{k}p &:= p_0 + p_3 \,\mathrm{sign}(k_3), \end{aligned} \tag{A.22}$$

and we denote

$$\sigma := \sqrt{t'^2 - \left(x'^i\right)^2 - z'^2} = -\frac{m}{\hat{k}p}. \tag{A.23}$$

We parametrize the product $\hat{k}p$ in (A.22) as $\hat{k}p = -\sqrt{\mathbf{p}^2 + m^2} + |\mathbf{p}|\cos\theta$, where $\cos\theta = \hat{\mathbf{k}}\mathbf{p}_0$. Apparently $\hat{k}p < 0$, and $t' > 0$ holds as well, which is equivalent to $h := p_0 - eA_0 + f < 0$. In fact, even $h \le -m$ is satisfied, since $h^2 \ge m^2$. This follows from (A.21) and the negativity of h, the latter is due to continuity in the coupling constant, since $h(e=0) = p_0 \le -m$. Thus, $t'(\varphi) > 0$, as $\hat{k}p$ is negative.

The kinetic momentum is defined by $p_\mu^{\mathrm{kin}} = S_{,\mu} - eA_\mu$, where $p_0^{\mathrm{kin}} = -E^{\mathrm{kin}} = -m\gamma$ and $p_i^{\mathrm{kin}} = m\dot{x}^i\gamma$, with the time-dependent Lorentz factor $\gamma = 1/\sqrt{1-\upsilon^2}$. In φ parametrization, $p_{\mathrm{kin}}^\mu = m x'^\mu/\sigma$, with σ in (A.23). This follows from $S_{,i} = \partial L/\partial \dot{x}^i$ and $S_{,0} = -H$, with $H = \dot{x}^i \partial L/\partial \dot{x}^i - L$, so that $\mathrm{d}S/\mathrm{d}t = L$ and $L = -m/\gamma + eA_0 + eA_i\dot{x}^i$. We thus find $p_\mu^{\mathrm{kin}} = p_\mu - eA_\mu - f(\varphi)\hat{k}_\mu$, according to (A.2). In particular, $p_0^{\mathrm{kin}} = -mt'/\sigma$, and we can identify the Lorentz factor as $\gamma = t'/\sigma$ or

$$\gamma = -\frac{1}{m}\big(p_0 - eA_0 + f(\varphi)\big), \tag{A.24}$$

with $f(\varphi)$ in (A.3) and $p_0 = -E_0 = -\sqrt{p_i^2 + m^2}$. Clearly, $\gamma \ge 1$, as pointed out after (A.23). The kinetic 3-momentum $p_i^{\mathrm{kin}} = m\upsilon_i\gamma$ is obtained via $p_i^{\mathrm{kin}} = mx'^i/\sigma$ and $p_3^{\mathrm{kin}} = mz'/\sigma$, with (A.22) and (A.23) substituted. Alternatively, we may use $p_\mu^{\mathrm{kin}} = S_{,\mu} - eA_\mu$ with (A.8) and (A.13)–(A.15), to find

$$\begin{aligned} p_\mu^{\mathrm{kin}} = S_{,\mu} - eA_\mu &= p_\mu - e^2(A_2 + B_2)\omega\hat{k}_\mu \\ &\quad + e\big[(A_1\omega\hat{k}_\mu - a_\mu)\cos(\omega\varphi) \\ &\quad - (B_1\omega\hat{k}_\mu - b_\mu)\sin(\omega\varphi)\big] \\ &\quad - e^2\omega\hat{k}_\mu\big[(A_2 - B_2)\cos(2\omega\varphi) \\ &\quad - C_2\sin(2\omega\varphi)\big]. \end{aligned} \tag{A.25}$$

The coefficients A_i, B_i, and C_2 are given explicitly in (A.16), in terms of polarization vectors.

In the following, we discuss some special cases regarding initial conditions and polarization, and then calculate general orbits in plane waves of arbitrary polarization. To this end, we need the p_i derivatives of the action coefficients (A.16), which define the trajectories according to (A.18) and (A.19). The wave vector of the plane wave is $k_\mu = \omega\hat{k}_\mu$ with $\hat{k}_\mu = (-1, 0, 0, \mathrm{sign}(k_3))$. (The same sign convention is used in action (A.17).) We note the identities

$$\begin{aligned} \hat{k}p &= \mathrm{sign}(k_3)p_3 - E_0 = -E_0|\alpha|, \\ E_0|\alpha| - \alpha p_3 &= E_0\alpha^2, \end{aligned} \tag{A.26}$$

with $E_0 = \sqrt{p_i^2 + m^2}$ and α defined in (A.19). Thus, $(\hat{k}p)_{,i} = -p_i/E_0$ for $i = 1, 2$, and $(\hat{k}p)_{,3} = \alpha$. As for the field amplitudes a_μ and b_μ in (A.8), we put $a_0 = b_0 = 0$, by invoking gauge freedom. The Lorentz condition $ak = bk = 0$ requires $a_3 = b_3 = 0$. Under these conditions, the p_i derivatives of the first-order coefficients in (A.16) read

$$\begin{aligned} A_{1,i} &= \frac{1}{\omega E_0^2\alpha^2}\left(\frac{ap}{E_0}p_i - E_0|\alpha|a_i\right), \\ A_{1,3} &= -\frac{ap}{\omega E_0^2\alpha}, \end{aligned} \tag{A.27}$$

and the same holds for $B_{1,i}$, with a_μ replaced by b_μ. The p_i derivatives of the second-order coefficients are

$$A_{2,i} = \frac{a^2 p_i}{4\omega E_0^3\alpha^2}, \qquad A_{2,3} = -\frac{a^2}{4\omega E_0^2\alpha}, \tag{A.28}$$

and the same holds true for $B_{2,i}$ and $C_{2,i}$, with a^2 replaced by b^2 and $2ab$, respectively.

Appendix B: Orbits in circularly and elliptically polarized waves

Circular polarization implies the constraints $a^2 = b^2$ and $ab = 0$ on the amplitudes in (A.8) and (A.9), in addition to the gauge and Lorentz conditions, which allow one to put $a_0 = b_0 = 0$ and $a_3 = b_3 = 0$ as pointed out after (A.26). Thus, $A_2 = B_2$ and $C_2 = C_{2,i} = 0$ according to (A.16) and (A.28), so that the 2ω modes drop out in the action (A.14). We use real polarization vectors $a_\mu = (0, 0, a_2, 0)$ and $b_\mu = (0, b_1, 0, 0)$, where a_2 and b_1 can only differ by a sign defining right/left-handedness, and we put $|a_2| = |b_1| =: a_{\mathrm{cp}}$. Choosing $p_1 = p_2 = 0$ as initial conditions, we find $A_1 = B_1 = 0$ in (A.16), so that the Lorentz factor $\gamma = -p_0^{\mathrm{kin}}/m$ is constant, see (A.25). The trajectory obtained via (A.18) and (A.19) is a helix with axis along the wave vector, and can readily be parametrized by time, since $A_{1,3} = B_{1,3} = 0$ in (A.19), according to (A.27). If the initial conditions $p_1 = p_2 = 0$ are not met, the Lorentz factor is not any more constant, the helical axis is tilted away from the z axis, and the base curve (obtained by projecting the helix onto a plane orthogonal to the helical axis) is an ellipse. The general orbit in a circularly polarized plane wave reads, cf. (A.18) and (A.19),

$$\begin{aligned}
(x,y) &= \frac{p_i}{E_0}t - e^2(A_{2,i}+B_{2,i})\omega\varphi \\
&\quad + e\big(A_{1,i}\sin(\omega\varphi) + B_{1,i}\cos(\omega\varphi)\big), \\
z &= \operatorname{sign}(k_3)(\beta-1)\varphi \\
&\quad + \frac{e}{|\alpha|}\big(A_{1,3}\sin(\omega\varphi) + B_{1,3}\cos(\omega\varphi)\big), \\
t &= \beta\varphi + \frac{e}{\alpha}\big(A_{1,3}\sin(\omega\varphi) + B_{1,3}\cos(\omega\varphi)\big),
\end{aligned} \tag{B.1}$$

where

$$\beta := \frac{1}{|\alpha|} - \frac{e^2}{\alpha}(A_{2,3}+B_{2,3})\omega, \qquad \alpha = \operatorname{sign}(k_3) - \frac{p_3}{E_0}, \tag{B.2}$$

so that $|\alpha| = \operatorname{sign}(k_3)\alpha$.

B.1 Helical motion

Helical orbits arise if the particle is injected parallel or antiparallel to the wave vector of a circularly polarized wave, implying vanishing orthogonal initial momentum, $p_1 = p_2 = 0$. By making use of (A.27), (A.28), (B.1), and (B.2), we find the helix

$$\begin{aligned}
x &= -\operatorname{sign}(b_1)\frac{ea_{\mathrm{cp}}}{\omega E_0|\alpha|}\cos\frac{\omega t}{\beta}, \\
y &= -\operatorname{sign}(a_2)\frac{ea_{\mathrm{cp}}}{\omega E_0|\alpha|}\sin\frac{\omega t}{\beta}, \\
z &= \operatorname{sign}(k_3)\frac{\beta-1}{\beta}t, \qquad t = \beta\varphi.
\end{aligned} \tag{B.3}$$

Here, $E_0 = \sqrt{p_3^2 + m^2}$ and

$$\beta = \frac{2E_0^2|\alpha| + e^2a_{\mathrm{cp}}^2}{2E_0^2\alpha^2}, \tag{B.4}$$

where we made use of (B.2) and (A.26). α is defined in (B.2), and $a_{\mathrm{cp}} = |a_2| = |b_1|$ determines the amplitude of the plane wave (A.8). The longitudinal velocity along the helical z axis reads

$$\upsilon_{\parallel} = \operatorname{sign}(k_3)\frac{\beta-1}{\beta}, \qquad 1-\upsilon_{\parallel}^2 = \frac{e^2a_{\mathrm{cp}}^2 + m^2}{E_0^2\alpha^2\beta^2}, \tag{B.5}$$

where we made use of (B.3), (B.4), and (A.26). The transversal velocity component along the helical base circle (obtained by putting $z = 0$ in (B.3)) is

$$\upsilon_{\perp}^2 = \frac{e^2a_{\mathrm{cp}}^2}{E_0^2\alpha^2\beta^2}. \tag{B.6}$$

The pitch angle $0 \le \alpha_{\mathrm{p}} \le \pi$ is defined by $\upsilon_{\perp} = \upsilon\sin\alpha_{\mathrm{p}}$ and $\upsilon_{\parallel} = \upsilon\cos\alpha_{\mathrm{p}}$, where $\upsilon = \sqrt{\upsilon_{\perp}^2 + \upsilon_{\parallel}^2}$ is the helical velocity. The Lorentz factor is constant,

$$\gamma = \frac{2E_0^2|\alpha| + e^2a_{\mathrm{cp}}^2}{2mE_0|\alpha|}, \qquad 1-\upsilon^2 = \frac{m^2}{E_0^2\alpha^2\beta^2}. \tag{B.7}$$

B.2 Orbits with elliptic base curve in circularly polarized waves

Trajectory (B.1) is the general solution for arbitrary initial 3-momentum p_i in a circularly polarized plane wave. We substitute the coefficients (A.27) and (A.28), specialized to circular polarization with polarization vectors as defined before (B.1). Equation (B.4) defining β remains valid with $E_0 = \sqrt{p^2 + m^2}$ substituted, according to (B.2). We thus find

$$\begin{aligned}
x &= \frac{p_1}{E_0|\alpha|}\varphi - \operatorname{sign}(b_1)\frac{ea_{\mathrm{cp}}}{\omega E_0|\alpha|}\cos(\omega\varphi), \\
y &= \frac{p_2}{E_0|\alpha|}\varphi - \operatorname{sign}(a_2)\frac{ea_{\mathrm{cp}}}{\omega E_0|\alpha|}\sin(\omega\varphi), \\
z &= \operatorname{sign}(k_3)(\beta-1)\varphi - \frac{ea_{\mathrm{cp}}}{\omega E_0^2\alpha^2}\big[\operatorname{sign}(a_2k_3)p_2\sin(\omega\varphi) \\
&\quad + \operatorname{sign}(b_1k_3)p_1\cos(\omega\varphi)\big], \\
t &= \beta\varphi - \frac{ea_{\mathrm{cp}}}{\omega E_0^2\alpha^2}\big[\operatorname{sign}(a_2)p_2\sin(\omega\varphi) \\
&\quad + \operatorname{sign}(b_1)p_1\cos(\omega\varphi)\big],
\end{aligned} \tag{B.8}$$

which replaces trajectory (B.3) if the initial 3-momentum has a non-vanishing component orthogonal to the direction of wave propagation. The velocity components are $\upsilon_i = x'^i/t'$ and $\upsilon_3 = z'/t'$, see (A.20). The line element (A.23) reads $\sigma = m/(E_0|\alpha|)$, where we made use of (A.26), and the kinetic momentum is $p_{\mathrm{kin}}^{\mu} = E_0|\alpha|x'^{\mu}$, as pointed out in the discussion preceding (A.24) and (A.25). In this way, we find the Lorentz factor

$$\begin{aligned}
\gamma &= \frac{1}{\sqrt{1-\upsilon^2(\varphi)}} \\
&= \frac{2E_0^2|\alpha| + e^2a_{\mathrm{cp}}^2}{2mE_0|\alpha|} + \frac{ea_{\mathrm{cp}}}{mE_0|\alpha|}\big[\operatorname{sign}(b_1)p_1\sin(\omega\varphi) \\
&\quad - \operatorname{sign}(a_2)p_2\cos(\omega\varphi)\big].
\end{aligned} \tag{B.9}$$

The helical axis of trajectory (B.8) is $(p_1, p_2, E_0\alpha(\beta-1))$, and the orthogonal projection of the orbit (base curve) is an ellipse. The coordinate unit vectors in the (x, y, z) frame are denoted by $\mathbf{e}_k$. We introduce a coordinate system with the helical axis as coordinate axis. To this end, we define the vectors

$$\begin{aligned}
\hat{\mathbf{e}}_3 &:= \operatorname{sign}\bigl(k_3(\beta-1)\bigr)\bigl(p_1, p_2, E_0\alpha(\beta-1)\bigr),\\
\hat{\mathbf{e}}_1 &:= \operatorname{sign}\bigl(k_3(\beta-1)\bigr)(-p_2, p_1, 0),\\
\hat{\mathbf{e}}_2 &:= \mathbf{e}_3 - \frac{\hat{\mathbf{e}}_3(\hat{\mathbf{e}}_3\mathbf{e}_3)}{\hat{\mathbf{e}}_3^2}.
\end{aligned} \tag{B.10}$$

Their squares read

$$\begin{aligned}
|\hat{\mathbf{e}}_3|^2 &= p_1^2 + p_2^2 + E_0^2\alpha^2(\beta-1)^2\\
&= E_0^2\alpha^2\beta^2 - e^2a_{\mathrm{cp}}^2 - m^2,\\
|\hat{\mathbf{e}}_1|^2 &= p_1^2 + p_2^2 = E_0^2|\alpha|\bigl(2-|\alpha|\bigr) - m^2,
\end{aligned} \tag{B.11}$$

and $|\hat{\mathbf{e}}_2| = |\hat{\mathbf{e}}_1|/|\hat{\mathbf{e}}_3|$. The corresponding unit vectors $\hat{\mathbf{e}}_i/|\hat{\mathbf{e}}_i|$ are denoted by $\hat{\mathbf{e}}_{0,i}$, and constitute a right-handed orthonormal triad. In particular, $\hat{\mathbf{e}}_{0,3} = \hat{\mathbf{e}}_{0,1} \times \hat{\mathbf{e}}_{0,2}$, where $\hat{\mathbf{e}}_{0,1}$ is the unit vector of $\mathbf{e}_3 \times \hat{\mathbf{e}}_3$. The $\hat{\mathbf{e}}_{0,2}$ axis is chosen in the plane generated by $\mathbf{e}_3$ and $\hat{\mathbf{e}}_3$. The z component of $\hat{\mathbf{e}}_3$ is positive, and $\hat{\mathbf{e}}_3$ coincides with the helical axis. We denote the projections $x^k\mathbf{e}_k\hat{\mathbf{e}}_{0,i}$ of trajectory (B.8) onto the new coordinate unit vectors by $(\hat{x}, \hat{y}, \hat{z})$,

$$\begin{aligned}
\hat{x} &= -\frac{\operatorname{sign}(\beta-1)ea_{\mathrm{cp}}}{|\hat{\mathbf{e}}_1|\omega E_0\alpha}\bigl[\operatorname{sign}(a_2)p_1\sin(\omega\varphi)\\
&\quad - \operatorname{sign}(b_1)p_2\cos(\omega\varphi)\bigr],\\
\hat{y} &= \frac{\operatorname{sign}(k_3)ea_{\mathrm{cp}}}{|\hat{\mathbf{e}}_1||\hat{\mathbf{e}}_3|\omega E_0^2\alpha^2}\bigl[E_0^2\alpha^2(\beta-1)\\
&\quad - |\hat{\mathbf{e}}_1|^2\bigr]\bigl[\operatorname{sign}(a_2)p_2\sin(\omega\varphi) + \operatorname{sign}(b_1)p_1\cos(\omega\varphi)\bigr],\\
\hat{z} &= \frac{\operatorname{sign}(\beta-1)}{|\hat{\mathbf{e}}_3|E_0\alpha}\biggl\{|\hat{\mathbf{e}}_3|^2\varphi\\
&\quad - \frac{ea_{\mathrm{cp}}\beta}{\omega}\bigl[\operatorname{sign}(a_2)p_2\sin(\omega\varphi) + \operatorname{sign}(b_1)p_1\cos(\omega\varphi)\bigr]\biggr\}.
\end{aligned} \tag{B.12}$$

The coordinate time is given in (B.8), and the kinetic momentum is $\hat{p}^{\mu}_{\mathrm{kin}} = E_0|\alpha|\hat{x}'^{\mu}$. Trajectory (B.12) coincides with trajectory (B.8) in the limit $p_1 = 0$ and $p_2 \to -\operatorname{sign}(k_3(\beta-1))0$. (The sign determines whether zero is approached from the right or left.) We define the angle $0 \le \varphi_0 < 2\pi$ by

$$\sin\varphi_0 := \frac{\operatorname{sign}(a_2)p_1}{|\hat{\mathbf{e}}_1|}, \qquad \cos\varphi_0 := \frac{\operatorname{sign}(b_1)p_2}{|\hat{\mathbf{e}}_1|}, \tag{B.13}$$

and write trajectory (B.12) as

$$\begin{aligned}
\hat{x} &= \frac{\operatorname{sign}(\beta-1)ea_{\mathrm{cp}}}{\omega E_0\alpha}\cos(\omega\varphi+\varphi_0),\\
\hat{y} &= \frac{\operatorname{sign}(a_2b_1k_3)ea_{\mathrm{cp}}}{|\hat{\mathbf{e}}_3|\omega E_0^2\alpha^2}\\
&\quad \times\bigl[E_0^2\alpha^2(\beta-1) - |\hat{\mathbf{e}}_1|^2\bigr]\sin(\omega\varphi+\varphi_0),\\
\hat{z} &= \frac{\operatorname{sign}(\beta-1)}{|\hat{\mathbf{e}}_3|E_0\alpha}\biggl[|\hat{\mathbf{e}}_3|^2\varphi\\
&\quad - \frac{ea_{\mathrm{cp}}\beta|\hat{\mathbf{e}}_1|}{\omega}\operatorname{sign}(a_2b_1)\sin(\omega\varphi+\varphi_0)\biggr],\\
t &= \beta\varphi - \frac{ea_{\mathrm{cp}}|\hat{\mathbf{e}}_1|}{\omega E_0^2\alpha^2}\operatorname{sign}(a_2b_1)\sin(\omega\varphi+\varphi_0).
\end{aligned} \tag{B.14}$$

The absolute values $|\hat{\mathbf{e}}_1|$ and $|\hat{\mathbf{e}}_3|$ are explicit in (B.11), and β in (B.4). We drop φ_0 in the argument of the harmonics, as this merely amounts to adding integration constants to the coordinates. The Lorentz factor is $\gamma = t'/\sigma$, where

$$\sigma = \sqrt{t'^2 - \hat{x}'^2 - \hat{y}'^2 - \hat{z}'^2} = \frac{m}{E_0|\alpha|}, \tag{B.15}$$

which can readily be derived by making use of (A.23)–(A.26). Time averages are calculated as

$$\langle f\rangle = (2\varphi)^{-1}\int_{-\varphi}^{+\varphi} f\,\mathrm{d}\varphi, \tag{B.16}$$

with $\varphi \to \infty$. The averaged squared φ derivatives of trajectory (B.14) read

$$\begin{aligned}
\bigl\langle \hat{x}'^2\bigr\rangle &= \frac{e^2a_{\mathrm{cp}}^2}{2E_0^2\alpha^2},\\
\bigl\langle \hat{y}'^2\bigr\rangle &= \frac{e^2a_{\mathrm{cp}}^2}{2E_0^2\alpha^2}\frac{(E_0^2\alpha^2(\beta-1) - |\hat{\mathbf{e}}_1|^2)^2}{E_0^2\alpha^2|\hat{\mathbf{e}}_3|^2},\\
\bigl\langle \hat{z}'^2\bigr\rangle &= \frac{|\hat{\mathbf{e}}_3|^2}{E_0^2\alpha^2} + \frac{e^2a_{\mathrm{cp}}^2\beta^2|\hat{\mathbf{e}}_1|^2}{2E_0^2\alpha^2|\hat{\mathbf{e}}_3|^2},\\
\bigl\langle t'^2\bigr\rangle &= \beta^2 + \frac{e^2a_{\mathrm{cp}}^2|\hat{\mathbf{e}}_1|^2}{2E_0^4\alpha^4}.
\end{aligned} \tag{B.17}$$

Identity (B.15) also holds with these averages under the root. The averaged transversal and longitudinal velocity components (orthogonal and parallel to the helical axis) stated in (3.18) and (3.19) are assembled as

$$\upsilon_{\perp}^2 = \frac{\langle \hat{x}'^2\rangle + \langle \hat{y}'^2\rangle}{\langle t'^2\rangle}, \qquad \upsilon_{\parallel}^2 = \frac{\langle \hat{z}'^2\rangle}{\langle t'^2\rangle}. \tag{B.18}$$

When calculating $\upsilon_{\perp}^2$, we substitute the identity

$$\begin{aligned}
&\bigl(E_0^2\alpha^2(\beta-1) - |\hat{\mathbf{e}}_1|^2\bigr)^2\\
&\quad = E_0^2\alpha^2|\hat{\mathbf{e}}_3|^2 - \bigl(e^2a_{\mathrm{cp}}^2 + m^2\bigr)|\hat{\mathbf{e}}_1|^2
\end{aligned} \tag{B.19}$$

into the $\langle \hat{y}'^2\rangle$ average. The averaged Lorentz factor is $\gamma_{\mathrm{av}} = (1-\upsilon^2)^{-1/2}$ with $\upsilon^2 = \upsilon_\parallel^2 + \upsilon_\perp^2$, see (3.3). Equivalently, $\gamma_{\mathrm{av}} = \sqrt{\langle t'^2\rangle}/\sigma$ according to (B.15). The ultra-relativistic limit, $\gamma_{\mathrm{av}} \gg 1$, can be realized by large injection energy E_0 or large field amplitude a_{cp}.

B.3 Time averaging of Lissajous orbits in elliptically polarized waves

We turn to the general case, elliptical polarization. The polarization vectors of the plane wave (A.8) are $a_\mu = (0, a_1, a_2, 0)$ and $b_\mu = (0, b_1, b_2, 0)$, with real a_i and b_i, as mentioned after (A.26). We denote the squared absolute values of the 3-vectors by a^2 and b^2, their scalar product by ab, and the product with the initial 3-momentum by ap and bp. (Since the zeroth component of the polarization vectors vanishes, these products coincide with the corresponding scalar 4-vector products $a_\mu p^\mu$, etc.) The zeroth component has been gauged to zero, and the third spatial component vanishes due to the Lorentz condition. These real polarization vectors can be chosen orthogonal to each other by adding a constant to the phase φ in (A.8), which can otherwise be ignored. (A phase factor can be split off from $a - ib$ to make its square real.) However, we will not assume orthogonality. Equations (A.26)–(A.28) and (B.2) remain valid, and the definition of β in (B.4) applies as well, if we substitute $a_{\mathrm{cp}} := \sqrt{(a^2+b^2)/2}$. Hence,

$$\beta = \frac{1}{|\alpha|}\left(1 + \frac{e^2 a_{\mathrm{cp}}^2}{2E_0^2|\alpha|}\right), \qquad a_{\mathrm{cp}}^2 = \frac{a^2+b^2}{2}, \tag{B.20}$$

with α in (B.2). We can also use the coordinate vectors $\hat{\mathbf{e}}_i$ in (B.10) and (B.11) with this β.

The trajectories in a plane wave of arbitrary polarization are found quite analogously to (B.1), by means of (A.14), (A.18), and (A.19). The x and y coordinates read

$$\begin{aligned} x_i = {} & \left[\frac{p_i}{E_0}\beta - e^2(A_{2,i} + B_{2,i})\omega\right]\varphi \\ & + e\left(\frac{p_i}{E_0\alpha}A_{1,3} + A_{1,i}\right)\sin(\omega\varphi) \\ & + e\left(\frac{p_i}{E_0\alpha}B_{1,3} + B_{1,i}\right)\cos(\omega\varphi) \\ & - \frac{e^2}{2}\left[\frac{p_i}{E_0\alpha}(A_{2,3} - B_{2,3}) + (A_{2,i} - B_{2,i})\right]\sin(2\omega\varphi) \\ & - \frac{e^2}{2}\left(\frac{p_i}{E_0\alpha}C_{2,3} + C_{2,i}\right)\cos(2\omega\varphi). \end{aligned} \tag{B.21}$$

The φ parametrization of time is

$$\begin{aligned} t = {} & \beta\varphi + \frac{e}{\alpha}\big[A_{1,3}\sin(\omega\varphi) + B_{1,3}\cos(\omega\varphi)\big] \\ & - \frac{e^2}{2\alpha}\big[(A_{2,3} - B_{2,3})\sin(2\omega\varphi) \\ & + C_{2,3}\cos(2\omega\varphi)\big], \end{aligned} \tag{B.22}$$

and the z coordinate is obtained via $z = \mathrm{sign}(k_3)(t-\varphi)$, as pointed out after (A.19). We substitute the coefficients (A.27) and (A.28), and use the real polarization vectors defined at the beginning of this subsection to find the general orbit in an elliptically polarized wave,

$$x_i = \frac{p_i}{E_0|\alpha|}\varphi - \frac{e}{\omega E_0|\alpha|}\big[a_i\sin(\omega\varphi) + b_i\cos(\omega\varphi)\big], \tag{B.23}$$

$$\begin{aligned} t = {} & \beta\varphi - \frac{e}{\omega E_0^2\alpha^2}\big[ap\sin(\omega\varphi) + bp\cos(\omega\varphi)\big] \\ & + \frac{e^2}{8\omega E_0^2\alpha^2}\big[\big(a^2 - b^2\big)\sin(2\omega\varphi) \\ & + 2ab\cos(2\omega\varphi)\big], \end{aligned} \tag{B.24}$$

and $z(\varphi)$ as above.

The linear φ term in the x and y coordinates (B.23) can be removed by a rotation of the coordinate frame, $\mathbf{e}_i \to \hat{\mathbf{e}}_{0,i}$; the orthonormal triad $\hat{\mathbf{e}}_{0,i}$ is defined in (B.10) and (B.11). The space coordinates projected onto the new coordinate unit vectors $\hat{\mathbf{e}}_{0,i}$ are found by means of (A.26), (B.2), and (B.4),

$$\begin{aligned} \hat{x} = {} & \frac{\mathrm{sign}(\beta-1)e}{|\hat{\mathbf{e}}_1|\omega E_0\alpha}\big[(a_1p_2 - a_2p_1)\sin(\omega\varphi) \\ & + (b_1p_2 - b_2p_1)\cos(\omega\varphi)\big], \\ \hat{y} = {} & \frac{\mathrm{sign}(k_3)e}{|\hat{\mathbf{e}}_1||\hat{\mathbf{e}}_3|\omega E_0^2\alpha^2}\Big\{\big[E_0^2\alpha^2(\beta-1) \\ & - |\hat{\mathbf{e}}_1|^2\big]\big[ap\sin(\omega\varphi) + bp\cos(\omega\varphi)\big] \\ & + \frac{e}{8}|\hat{\mathbf{e}}_1|^2\big[\big(a^2 - b^2\big)\sin(2\omega\varphi) \\ & + 2ab\cos(2\omega\varphi)\big]\Big\}, \\ \hat{z} = {} & \frac{\mathrm{sign}(\beta-1)}{|\hat{\mathbf{e}}_3|E_0\alpha}\Big\{|\hat{\mathbf{e}}_3|^2\varphi - \frac{e}{\omega}\beta\big[ap\sin(\omega\varphi) + bp\cos(\omega\varphi)\big] \\ & + \frac{e^2}{8\omega}(\beta-1)\big[\big(a^2 - b^2\big)\sin(2\omega\varphi) + 2ab\cos(2\omega\varphi)\big]\Big\}. \end{aligned} \tag{B.25}$$

Trajectories (B.25) are the counterpart to (B.12) in a plane wave of arbitrary polarization. Their base curve, obtained by projecting the helix onto the plane orthogonal to the helical axis $\hat{\mathbf{e}}_3$, is a closed Lissajous figure. The φ parametrization of time is given in (B.24). The time-averaged squares of the

φ derivatives are calculated via (B.16),

$$\begin{aligned}
\langle \hat{x}'^2\rangle &= \frac{e^2}{2E_0^2\alpha^2|\hat{\mathbf{e}}_1|^2}\big((a_1p_2-a_2p_1)^2+(b_1p_2-b_2p_1)^2\big),\\
\langle \hat{y}'^2\rangle &= \frac{e^2}{2E_0^2\alpha^2|\hat{\mathbf{e}}_1|^2}\frac{(E_0^2\alpha^2(\beta-1)-|\hat{\mathbf{e}}_1|^2)^2}{E_0^2\alpha^2|\hat{\mathbf{e}}_3|^2}\big((ap)^2+(bp)^2\big)\\
&\quad+\frac{e^4|\hat{\mathbf{e}}_1|^2}{32E_0^4\alpha^4|\hat{\mathbf{e}}_3|^2}\big((a^2-b^2)^2+4(ab)^2\big),\\
\langle \hat{z}'^2\rangle &= \frac{|\hat{\mathbf{e}}_3|^2}{E_0^2\alpha^2}+\frac{e^2\beta^2}{2E_0^2\alpha^2|\hat{\mathbf{e}}_3|^2}\big((ap)^2+(bp)^2\big)\\
&\quad+\frac{e^4(\beta-1)^2}{32E_0^2\alpha^2|\hat{\mathbf{e}}_3|^2}\big((a^2-b^2)^2+4(ab)^2\big),\\
\langle t'^2\rangle &= \beta^2+\frac{e^2}{2E_0^4\alpha^4}\big((ap)^2+(bp)^2\big)\\
&\quad+\frac{e^4}{32E_0^4\alpha^4}\big((a^2-b^2)^2+4(ab)^2\big).
\end{aligned}\tag{B.26}$$

The averages (B.17) are recovered by putting $|a_2|=|b_1|=a_{\rm cp}$ and $a_1=b_2=0$. The line element is assembled as in (B.15),

$$\sigma^2=\langle t'^2\rangle-\langle \hat{x}'^2\rangle-\langle \hat{y}'^2\rangle-\langle \hat{z}'^2\rangle=\frac{m^2}{E_0^2\alpha^2},\tag{B.27}$$

where we used the identity $(a_1p_2-a_2p_1)^2+(ap)^2=a^2|\hat{\mathbf{e}}_1|^2$, which follows from (B.11), and the same for b. In (3.20), we also need the averaged coordinate squares of the Lissajous orbits, obtained as $\langle \hat{x}^2\rangle=\langle \hat{x}'^2\rangle/\omega^2$ and $\langle \hat{y}^2\rangle=\langle \hat{y}'^2, 32\to 128\rangle/\omega^2$. (As for the latter, the factor 32 in the denominator of the second term of $\langle \hat{y}'^2\rangle$ in (B.26) is replaced by 128.) The time-averaged Lorentz factor (3.3) reads

$$\gamma_{\rm av}=\sqrt{\langle t'^2\rangle}/\sigma.\tag{B.28}$$

The tachyonic radiation densities calculated in Sect. 3 and Appendix C are based on these time averages.

Appendix C: Polarization triads and ultra-relativistic power asymptotics

In (2.4), we use two real transversal polarization vectors $\boldsymbol{\varepsilon}_{1,2}$, so that $\boldsymbol{\varepsilon}_1$, $\boldsymbol{\varepsilon}_2$, and $\mathbf{n}:=\mathbf{x}/|\mathbf{x}|$ constitute an orthonormal triad. We choose $\boldsymbol{\varepsilon}_1$ orthogonal to $\mathbf{n}$ and the coordinate unit vector $\mathbf{e}_3$, and place $\boldsymbol{\varepsilon}_2$ in the plane generated by $\mathbf{n}$ and $\mathbf{e}_3$,

$$\boldsymbol{\varepsilon}_1=\frac{\mathbf{e}_3\times\mathbf{n}}{\sqrt{1-(\mathbf{n}\mathbf{e}_3)^2}},\qquad \boldsymbol{\varepsilon}_2=\frac{\mathbf{e}_3-\mathbf{n}(\mathbf{n}\mathbf{e}_3)}{\sqrt{1-(\mathbf{n}\mathbf{e}_3)^2}},\tag{C.1}$$

so that $\mathbf{n}=\boldsymbol{\varepsilon}_1\times\boldsymbol{\varepsilon}_2$. Occasionally, we will write $\boldsymbol{\varepsilon}_3$ for $\mathbf{n}$, so that the real unit vectors $\boldsymbol{\varepsilon}_i$ define a right-handed triad. As for the angular parametrization, we use

$$\begin{aligned}
&\boldsymbol{\varepsilon}_3\mathbf{e}_1=\cos\varphi\sin\theta,\qquad \boldsymbol{\varepsilon}_3\mathbf{e}_2=\sin\varphi\sin\theta,\\
&\boldsymbol{\varepsilon}_3\mathbf{e}_3=\cos\theta,\qquad \boldsymbol{\varepsilon}_1\mathbf{e}_1=-\sin\varphi,\\
&\boldsymbol{\varepsilon}_1\mathbf{e}_2=\cos\varphi,\qquad \boldsymbol{\varepsilon}_1\mathbf{e}_3=0,\\
&\boldsymbol{\varepsilon}_2\mathbf{e}_1=-\cos\theta\cos\varphi,\qquad \boldsymbol{\varepsilon}_2\mathbf{e}_2=-\cos\theta\sin\varphi,\\
&\boldsymbol{\varepsilon}_2\mathbf{e}_3=\sin\theta.
\end{aligned}\tag{C.2}$$

The $\mathbf{e}_{1,2,3}$ are Cartesian coordinate unit vectors. We may write the vectors $\boldsymbol{\xi}_{m=-1,0,1}$ (employed in the decomposition of the phase in (2.10)) in a coordinate basis as $\xi_{m,i}\mathbf{e}_i$, so that the angular parametrization of $\boldsymbol{\varepsilon}_3\boldsymbol{\xi}_m$ required in the coefficients $\alpha_{m=-1,0,1}$ (defined in (2.11)) is obtained via $\xi_{m,i}\boldsymbol{\varepsilon}_3\mathbf{e}_i$.

We turn to the ultra-relativistic steepest-descent asymptotics of the power coefficients (2.25). As mentioned after (3.9), the stationary point of $2|\alpha_1|$ in the argument of the Bessel functions in the flux coefficients (2.23) is located at $\cos\theta_{\rm c}\sim\upsilon_\parallel$ if we use the angular parametrization (3.7) of α_1. We expand at $\theta_{\rm c}$,

$$2|\alpha_1|=\frac{n\tilde{\omega}}{\tilde{\beta}}\frac{R}{\sqrt{1-\upsilon_\parallel^2}}\left(1+\frac{m_{\rm t}^2}{2}\frac{\tilde{\beta}^2}{n^2\tilde{\omega}^2}(1-\upsilon_\parallel^2)\right.\\
\left.-\frac{1}{2}\frac{(\theta-\theta_{\rm c})^2}{1-\upsilon_\parallel^2}+\cdots\right),\tag{C.3}$$

and write the argument in the Airy functions (2.26) as

$$\lambda=2^{1/3}n^{2/3}\left(1-\frac{\tilde{\omega}R}{\tilde{\beta}}\frac{1}{\sqrt{1-\upsilon_\parallel^2}}-\frac{m_{\rm t}^2\tilde{\beta}R}{2\tilde{\omega}n^2}\sqrt{1-\upsilon_\parallel^2}\right.\\
\left.+\frac{1}{2}\frac{\tilde{\omega}R}{\tilde{\beta}}\frac{(\theta-\theta_{\rm c})^2}{(1-\upsilon_\parallel^2)^{3/2}}+\cdots\right).\tag{C.4}$$

In terms of the velocity component along the base circle (obtained by putting $z=0$ in (3.1)) and the averaged Lorentz factor (3.3), this reads

$$\lambda=\frac{n^{2/3}}{2^{2/3}\upsilon_\perp^2}\left(\frac{1}{\gamma_{\rm av}^2}-\frac{m_{\rm t}^2\upsilon_\perp^4\tilde{\beta}^2}{\tilde{\omega}^2n^2}+(\theta-\theta_{\rm c})^2+\cdots\right).\tag{C.5}$$

The pitch angle is defined in (3.4); at this juncture, we can approximate $\upsilon_\perp\sim\sin\alpha_{\rm p}$ (as pointed out after (3.22)), and introduce a new integration variable ψ in the power coefficients,

$$\psi=\frac{\theta-\theta_{\rm c}}{\varepsilon},\qquad \varepsilon:=\sqrt{\frac{1}{\gamma_{\rm av}^2}-\frac{m_{\rm t}^2\tilde{\beta}^2\sin^4\alpha_{\rm p}}{\tilde{\omega}^2n^2}},\tag{C.6}$$

to be substituted into (C.3) and (C.5). In the Airy functions (2.26), we can thus use

$$\lambda = \tilde{\eta}\bigl(1+\psi^2\bigr), \qquad \tilde{\eta} := \frac{n^{2/3}\varepsilon^2}{2^{2/3}\sin^2\alpha_{\mathrm{p}}}. \tag{C.7}$$

The solid-angle element in (2.25) can be approximated by $\sin\theta\,\mathrm{d}\theta \sim \varepsilon\sin\alpha_{\mathrm{p}}\,\mathrm{d}\psi$, since $\sin\theta_{\mathrm{c}} \sim \upsilon_\perp \sim \sqrt{1-\upsilon_\parallel^2}$.

We calculate the amplitudes $A^{(j)}(\omega_n^+, n)$ and $B^{(j)}(\omega_n^+)$ in (2.17) by expanding at the stationary phase θ_{c}. For instance, in (3.7), $\alpha_{1,\mathrm{Re}} \sim (n/2)\cos\varphi$ and $\alpha_{1,\mathrm{Im}} \sim (n/2)\sin\varphi$, and thus $|\alpha_1| \sim n/2$. As θ_{c} is the stationary point, there is no linear dependence on $\theta-\theta_{\mathrm{c}}$. In the amplitudes (2.17), we use the polarization vectors (C.1) and their angular parametrization (C.2). [The unit vectors $\mathbf{e}_i$ are identified with $\hat{\mathbf{e}}_{i,0}$, since the coordinates of helix (3.1) refer to $\hat{\mathbf{e}}_{i,0}$, as does trajectory (B.25).] The φ dependence of the vector products in (C.2) drops out in the amplitudes, and the polar-angle dependence is expanded at the critical point, $\sin\theta \sim \sin\alpha_{\mathrm{p}} + \varepsilon\psi\cos\alpha_{\mathrm{p}}$ and $\cos\theta \sim \cos\alpha_{\mathrm{p}} - \varepsilon\psi\sin\alpha_{\mathrm{p}}$. In this way, we obtain

$$\begin{aligned} &A^{(1)}(\omega_n^+) = \mathrm{O}(\psi^4), \qquad A^{(2)} \sim \tilde{\beta}^2\varepsilon^2\psi^2, \qquad A^{(3)} \sim \tilde{\beta}^2, \\ &B^{(1)}(\omega_n^+) \sim R^2\tilde{\omega}^2 \sim \tilde{\beta}^2\sin^2\alpha_{\mathrm{p}}, \qquad B^{(2)} \sim B^{(3)} = \mathrm{O}(\psi^4). \end{aligned} \tag{C.8}$$

By making use of the Nicholson asymptotics (2.26), we find the ultra-relativistic limit of the flux coefficients (2.23) as

$$\begin{aligned} S_n^{\mathrm{T}(1)} &\sim \frac{2^{4/3}}{n^{4/3}}\frac{n^2\tilde{\omega}^2}{\sin^4\alpha_{\mathrm{p}}}\frac{n^2\tilde{\omega}^2\mathrm{Ai}'^2(\lambda)}{n^2\tilde{\omega}^2 + m_{\mathrm{t}}^2\tilde{\beta}^2\sin^4\alpha_{\mathrm{p}}}, \\ S_n^{\mathrm{T}(2)} &\sim \frac{2^{2/3}}{n^{2/3}}\frac{n^2\tilde{\omega}^2}{\sin^6\alpha_{\mathrm{p}}}\frac{n^2\tilde{\omega}^2\varepsilon^2\psi^2\mathrm{Ai}^2(\lambda)}{n^2\tilde{\omega}^2 + m_{\mathrm{t}}^2\tilde{\beta}^2\sin^4\alpha_{\mathrm{p}}}, \\ S_n^{\mathrm{L}} &\sim \frac{2^{2/3}}{n^{2/3}}\frac{\tilde{\beta}^2}{\sin^2\alpha_{\mathrm{p}}}\frac{n^2\tilde{\omega}^2\mathrm{Ai}^2(\lambda)}{n^2\tilde{\omega}^2 + m_{\mathrm{t}}^2\tilde{\beta}^2\sin^4\alpha_{\mathrm{p}}}, \end{aligned} \tag{C.9}$$

with argument λ in (C.7). The asymptotic power coefficients (2.25) are assembled as

$$\begin{aligned} P_n^{\mathrm{T}(j)} &\sim \frac{q^2}{4\pi^2}\frac{\varepsilon\sin\alpha_{\mathrm{p}}}{\beta^2}\int_{-\infty}^{+\infty} S_n^{\mathrm{T}(j)}\,\mathrm{d}\psi, \\ P_n^{\mathrm{L}} &\sim \frac{q^2}{4\pi^2}\frac{\varepsilon\sin\alpha_{\mathrm{p}}}{\beta^2}m_{\mathrm{t}}^2\int_{-\infty}^{+\infty} S_n^{\mathrm{L}}\,\mathrm{d}\psi. \end{aligned} \tag{C.10}$$

Here, the integrals over the squared Airy functions in (C.9) can be replaced by handier (anti-)derivatives [31],

$$\begin{aligned} &\sqrt{\tilde{\eta}}\int_{-\infty}^{+\infty}\mathrm{Ai}^2\bigl(\tilde{\eta}(1+\psi^2)\bigr)\,\mathrm{d}\psi = \frac{1}{2}\int_\eta^\infty \mathrm{Ai}(x)\,\mathrm{d}x, \\ &\sqrt{\tilde{\eta}}\int_{-\infty}^{+\infty}\mathrm{Ai}^2\bigl(\tilde{\eta}(1+\psi^2)\bigr)\psi^2\,\mathrm{d}\psi \\ &\quad = -\frac{1}{4}\biggl(\int_\eta^\infty \mathrm{Ai}(x)\,\mathrm{d}x + \frac{\mathrm{Ai}'(\eta)}{\eta}\biggr), \\ &\frac{1}{\sqrt{\tilde{\eta}}}\int_{-\infty}^{+\infty}\mathrm{Ai}'^2\bigl(\tilde{\eta}(1+\psi^2)\bigr)\,\mathrm{d}\psi \\ &\quad = -\frac{1}{4}\biggl(\int_\eta^\infty \mathrm{Ai}(x)\,\mathrm{d}x + 3\frac{\mathrm{Ai}'(\eta)}{\eta}\biggr), \end{aligned} \tag{C.11}$$

where we use $\eta := 2^{2/3}\tilde{\eta}$ as spectral variable, with $\tilde{\eta}$ in (C.7). This also gives the analytic continuation to negative η, see (3.11).

References

1. S. Tanaka, Prog. Theor. Phys. **24**, 171 (1960)
2. R. Newton, Science **167**, 1569 (1970)
3. G. Feinberg, Sci. Am. **222**(2), 69 (1970)
4. C. Baltay, G. Feinberg, N. Yeh, R. Linsker, Phys. Rev. D **1**, 759 (1970)
5. R. Tomaschitz, Eur. Phys. J. B **17**, 523 (2000)
6. R. Tomaschitz, Physica A **335**, 577 (2004)
7. R. Tomaschitz, Eur. Phys. J. C **49**, 815 (2007)
8. A.V. Bessarab, A.A. Gorbunov, S.P. Martynenko, N.A. Prudkoy, IEEE Trans. Plasma Sci. **32**, 1400 (2004)
9. A.V. Bessarab, S.P. Martynenko, N.A. Prudkoi, A.V. Soldatov, V.A. Terekhin, Radiat. Phys. Chem. **75**, 825 (2006)
10. M.S. Bigelow, N.N. Lepeshkin, R.W. Boyd, Science **301**, 200 (2003)
11. T. Baba, Nat. Photon. **2**, 465 (2008)
12. G.M. Gehring, A. Schweinsberg, C. Barsi, N. Kostinski, R.W. Boyd, Science **312**, 895 (2006)
13. L. Thévenaz, Nat. Photon. **2**, 474 (2008)
14. G. Dolling, C. Enkrich, M. Wegener, C.M. Soukoulis, S. Linden, Science **312**, 892 (2006)
15. Y.I. Salamin, S.X. Hu, K.Z. Hatsagortsyan, C.H. Keitel, Phys. Rep. **427**, 41 (2006)
16. G.A. Mourou, T. Tajima, S.V. Bulanov, Rev. Mod. Phys. **78**, 309 (2006)
17. R. Tomaschitz, Ann. Phys. **322**, 677 (2007)
18. R. Tomaschitz, Physica A **387**, 3480 (2008)
19. R. Tomaschitz, Physica B **404**, 1383 (2009)
20. R. Tomaschitz, Opt. Commun. **282**, 1710 (2009)
21. A. Pukhov, Rep. Prog. Phys. **66**, 47 (2003)
22. E. Esarey, C.B. Schroeder, W.P. Leemans, Rev. Mod. Phys. **81**, 1229 (2009)
23. R. Tomaschitz, Eur. Phys. J. C (2010). doi:10.1140/epjc/s10052-010-1401-8
24. F. Aharonian, A.G. Akhperjanian, U. Barres de Almeida, A.R. Bazer-Bachi, B. Behera, M. Beilicke et al., Astron. Astrophys. **481**, L103 (2008)
25. V.A. Acciari, E. Aliu, T. Arlen, M. Beilicke, W. Benbow, M. Böttcher et al., Astrophys. J. **693**, L104 (2009)
26. E. Aliu, H. Anderhub, L.A. Antonelli, P. Antoranz, M. Backes, C. Baixeras et al., Astrophys. J. **692**, L29 (2009)
27. R. Tomaschitz, Physica A **385**, 558 (2007)
28. R. Tomaschitz, EPL **84**, 19001 (2008)
29. W. Magnus, F. Oberhettinger, R.P. Soni, *Formulas and Theorems for the Special Functions of Mathematical Physics* (Springer, New York, 1966)
30. M. Abramowitz, I.A. Stegun, *Handbook of Mathematical Functions* (Dover, New York, 1972)
31. D.E. Aspnes, Phys. Rev. **147**, 554 (1966)
32. S. Ichimaru, Rev. Mod. Phys. **65**, 255 (1993)
33. U. Teubner, P. Gibbon, Rev. Mod. Phys. **81**, 445 (2009)
34. A. Minguzzi, M.P. Tosi, Physica B **300**, 27 (2001)

35. R. Tomaschitz, Phys. Lett. A **366**, 289 (2007)
36. R. Tomaschitz, Phys. Lett. A **372**, 4344 (2008)
37. J.A. Wheeler, R.P. Feynman, Rev. Mod. Phys. **17**, 157 (1945)
38. F. Hoyle, J.V. Narlikar, Rev. Mod. Phys. **67**, 113 (1995)
39. R. Tomaschitz, Class. Quantum Gravity **18**, 4395 (2001)
40. G.N. Plass, Rev. Mod. Phys. **33**, 37 (1961)
41. J. Rafelski, L. Labun, Y. Hadad, AIP Conf. Proc. **1228**, 39 (2009)
42. Y. Hadad, L. Labun, J. Rafelski, N. Elkina, C. Klier, H. Ruhl, arXiv:1005.3980
43. P.A.M. Dirac, Proc. R. Soc. Lond. A **257**, 32 (1960)
44. V.B. Berestetskii, E.M. Lifshitz, L.P. Pitaevskii, *Quantum Electrodynamics* (Pergamon, Oxford, 1982)
45. A.A. Abdo, M. Ackermann, M. Ajello, W.B. Atwood, M. Axelsson, L. Baldini et al., Astrophys. J. **707**, 1310 (2009)
46. R. Tomaschitz, EPL **85**, 29001 (2009)
47. T. Lindner, D.S. Hanna, J. Kildea, J. Ball, D.A. Bramel, J. Carson et al., Astropart. Phys. **28**, 338 (2007)
48. D. Horan, H.M. Badran, I.H. Bond, P.J. Boyle, S.M. Bradbury, J.H. Buckley et al., Astrophys. J. **603**, 51 (2004)
49. F. Aharonian, A. Akhperjanian, M. Beilicke, K. Bernlöhr, H.-G. Börst, H. Bojahr et al., Astron. Astrophys. **421**, 529 (2004)
50. R. Tomaschitz, Physica B **405**, 1022 (2010)
51. R. Tomaschitz, EPL **89**, 39002 (2010)
52. R. Tomaschitz, J. Phys. A **38**, 2201 (2005)
53. R. Tomaschitz, Eur. Phys. J. C **45**, 493 (2006)
54. J.H. Eberly, A. Sleeper, Phys. Rev. **176**, 1570 (1968)
55. E.S. Sarachik, G.T. Schappert, Phys. Rev. D **1**, 2738 (1970)
56. A.A. Sokolov, I.M. Ternov, *Radiation from Relativistic Electrons* (Hilger, Bristol, 1986)